the plant journal

SEB SOCIETY FOR EXPERIMENTAL BIOLOGY

The Plant Journal (2025) **122,** e70225 doi: 10.1111/tpj.70225

Nucleobase-ascorbate transporter *OsNAT9* regulates seed vigor and drought tolerance by modulating ascorbic acid homeostasis in rice

Sufeng Liao[1,2,3], Kunyang Li[1,2,3], Yidong Wei[2,3], Shuai Zhao[1], Min Zhang[1,2,3], Jinlan Wang[2,3], Jiahuan Jiang[2,3], Ting Chen[1,2,3], Fangxi Wu[2,3], Jiaxing Fan[1,2,3], Qiuhua Cai[2,3], Yingheng Wang[2,3], Liping Chen[2,3], Wei He[2,3], Huaan Xie[1,2,3,*] and Jianfu Zhang[1,2,3,*]

[1]*Cross-Straits Agricultural Technology Cooperation Center under the Ministry of Agriculture and Rural Affairs, College of Agriculture, Fujian Agriculture and Forestry University, Fuzhou 350002, China,*

[2]*Rice Research Institute, Fujian Academy of Agricultural Sciences, Fuzhou 350018, China, and*

[3]*State Key Laboratory of Ecological Pest Control for Fujian and Taiwan Crops/Key Laboratory of Germplasm Innovation and Molecular Breeding of Hybrid Rice for South China, Ministry of Agriculture and Affairs, P.R. China/Incubator of National Key Laboratory of Germplasm Innovation and Molecular Breeding between Fujian and Ministry of Sciences and Technology/Fuzhou Branch, National Rice Improvement Center of China/Fujian Engineering Laboratory of Crop Molecular Breeding/Fujian Key Laboratory of Rice Molecular Breeding, Fuzhou 350003, China*

Received 30 September 2024; revised 24 April 2025; accepted 5 May 2025.
*For correspondence (e-mail jianfzhang@163.com and huaanxie@163.com).

SUMMARY

Drought and seed aging severely impact crop yield and seed vigor, respectively. Here, we identified the rice protein OsNAT9, a nucleobase–ascorbate transporter, as being crucial for seed vigor and drought tolerance. Knockout of *OsNAT9* resulted in a significant reduction in seed vigor; however, the application of exogenous ascorbic acid (AsA) and the breaking of seed dormancy restored this phenotype, suggesting that *OsNAT9* regulates seed vigor by modulating seed dormancy. Furthermore, the *Osnat9* mutants exhibited decreased AsA concentration in the endosperm, impairing the scavenging of reactive oxygen species (ROS) in aged seeds, which disrupted starch structure and seed vigor. During the aging process, both the knockout and overexpression of *OsNAT9* affected AsA efflux, disrupting the redox homeostasis of AsA pools, increasing ROS accumulation, and ultimately reducing embryo vigor. In addition, the *Osnat9* mutants displayed reduced drought tolerance, accompanied by decreased AsA concentration and increased ROS accumulation, whereas *OsNAT9*-overexpressed lines showed the opposite phenotypes. The OsNAT9 protein exhibited either a uniform or punctate distribution on the cytomembrane. Protoplast secretion assays and microscale thermophoresis experiments further confirmed that OsNAT9 functions as a cytomembrane-localized efflux transporter responsible for AsA secretion. This study highlights the dual role of *OsNAT9* in regulating seed vigor and drought tolerance by maintaining the homeostasis of AsA pools and reducing ROS accumulation. These findings provide novel insights into AsA efflux transport and its implications for seed vigor and stress adaptation. Furthermore, this study identifies *OsNAT9* as a potential target for enhancing crop stress tolerance and seed longevity.

Keywords: *Oryza sativa* L., ascorbic acid, efflux transporter, seed vigor, aging, drought, reactive oxygen species.

INTRODUCTION

Seed vigor is an important index for evaluating seed quality and predicting potential crop yield, and it plays a vital role in determining seed storability (Zhao et al., 2018). During storage, seeds undergo an irreversible decline or, in severe cases, a complete loss of vitality, a process known as deterioration or aging (Chhabra & Singh, 2019). The free radical theory is one of the most widely accepted explanations for the processes underlying seed aging (Ziada et al., 2020). Throughout the aging process, mitochondrial respiration and cytomembrane-localized respiratory burst oxidase homologs (RBOH) contribute to the accumulation of reactive oxygen species (ROS), which, in turn, induce oxidative damage in lipids, proteins, and nucleic acids,

thereby accelerating the aging process (Ye et al., 2024). Seed aging and drought stress both lead to the accumulation of ROS within cells, causing oxidative damage (Wang, Xu, et al., 2023). In response, plants have evolved complex antioxidant defense mechanisms (including enzymatic and non-enzymatic antioxidants) to mitigate the effects of ROS and protect cellular components from oxidative stress damage (Singh et al., 2024).

Ascorbic acid (AsA), a vital redox compound abundant in plants, plays multifaceted roles in growth, development, and stress adaptation (Akram et al., 2017; Pignocchi & Foyer, 2003). AsA functions as an efficient ROS scavenger, mitigating ROS through enzymatic and non-enzymatic pathways (Celi et al., 2023; Foyer & Halliwell, 1976; Padh, 1990). Within the apoplast, AsA is considered the sole antioxidant buffer, crucial for maintaining redox homeostasis (Celi et al., 2023; Pignocchi & Foyer, 2003). Furthermore, AsA plays a critical role in the regulation of cell division and differentiation. Research indicates that AsA is required for the transition of the cell cycle from the G1 phase to the S phase (Kerk & Feldman, 1995; Pignocchi & Foyer, 2003). In maize root tips, an increase in ascorbate oxidase accumulation within the quiescent center results in reduced AsA levels, causing these cells to predominantly remain in an extended G1 phase. Conversely, the application of exogenous AsA facilitates the quiescent center proceeding to mitosis (Kerk & Feldman, 1995, Pignocchi & Foyer, 2003). In *Arabidopsis*, the *DEFECTIVE IN TAPETAL DEVELOPMENT AND FUNCTION1* gene modulates the balance between cell division and differentiation in the tapetum by regulating the expression of genes involved in AsA biosynthesis and oxidation (Wu et al., 2023). Additionally, AsA is critical for the regulation of cell wall lignification. Under stress conditions, such as pathogen infection or mechanical injury, apoplastic AsA is rapidly oxidized to form dehydroascorbic acid (DHA), which initiates lignin polymerization and enhances cell wall resistance to pathogens (Horemans et al., 2000; Pignocchi & Foyer, 2003).

In plants, the source of AsA is primarily from the *de novo* biosynthesis pathway and the recycling pathway (Wheeler et al., 1998). The *de novo* biosynthesis pathway predominantly depends on the D-mannose/L-galactose pathway, wherein VITAMIN C DEFECTIVE1 (VTC1) serves as the rate-limiting enzyme (Conklin et al., 1996; Ishikawa et al., 2018; Wheeler et al., 1998). In *Arabidopsis*, the *vtc1* mutant contains only 25%–30% of the AsA concentrations observed in the wild-type plant due to defective AsA biosynthesis (Conklin et al., 1997; Conklin et al., 1999). The AsA recycling pathway relies on the ascorbate–glutathione cycle. Within this cycle, ascorbate peroxidase catalyzes the oxidation of AsA to monodehydroascorbate (MDHA) and DHA using hydrogen peroxide (Mittler, 2002; Pignocchi & Foyer, 2003). Subsequently, MDHA reductase (MDHAR) and DHA reductase (DHAR) regenerate AsA from MDHA and DHA, utilizing NAD(P)H and glutathione (GSH), respectively, thus constituting the AsA oxidation–reduction system (Foyer & Noctor, 2011; Gallie, 2013; Pignocchi & Foyer, 2003). The *de novo* biosynthesis and recycling pathways operate synergistically to maintain the homeostasis of AsA pools and redox equilibrium across various cellular compartments (Broad et al., 2020; Chen et al., 2020; Yu et al., 2019; Zhang et al., 2009). Nonetheless, the regulatory mechanisms governing the homeostasis of AsA pools under stress conditions are inadequately understood.

The redox state of AsA pools is strictly regulated across various cellular compartments, including the apoplast. The majority of enzymatic reactions involved in AsA biosynthesis occur within the cytoplasm, whereas the final step is catalyzed by L-galactose-1,4-lactone dehydrogenase on the inner mitochondrial membrane (Wheeler et al., 1998; Zhou et al., 2018). This process necessitates the translocation of AsA across the mitochondrial membrane. Given the absence of reducing agents such as NADPH in the apoplast, plant cells must regulate the redox state of the apoplast by absorbing DHA and secreting AsA (Ishikawa et al., 2018; Pignocchi & Foyer, 2003). Generally, AsA and its oxidized form, DHA, are considered incapable of freely diffusing through the phospholipid bilayer under physiological pH conditions, thereby necessitating specific transporters to facilitate their movement between different cellular compartments (Horemans et al., 2000; Pignocchi & Foyer, 2003). Two AsA transporters have been identified in plants, namely, AtPHT4;4 and AtDTX25 (Hoang et al., 2021; Miyaji et al., 2015; Tóth et al., 2024). AtPHT4;4 is localized to the chloroplast envelope and mediates AsA influx into chloroplasts, which is essential for tolerance to high-light stress (Miyaji et al., 2015). AtDTX25 is localized to the vacuolar membrane and plays a role in the reduction and remobilization of Fe^{3+} within vacuoles (Hoang et al., 2021). In mammals, the nucleobase–ascorbate transporter (NAT) family members SVCT1 and SVCT2 facilitate the uptake and intracellular distribution of AsA (Wang, He, et al., 2023). However, the identity of the cytomembrane-localized AsA transporter in plants has remained elusive. In plants, although the maize Leaf Permease1 (LPE1), a member of the NAT family, binds to AsA, its functional expression in the filamentous fungus *Aspergillus nidulans* does not exhibit AsA absorption activity (Argyrou et al., 2001). Thus, the specific NAT family members responsible for AsA transport in plants have still to be identified.

In this study, we identified OsNAT9 in rice as a cytomembrane-localized AsA transporter that directly binds AsA and facilitates its efflux. Notably, OsNAT9 plays dual roles in regulating seed vigor and drought tolerance in rice. Knockout of OsNAT9 resulted in decreased AsA levels, increased ROS accumulation in the endosperm, and disruption of endosperm structure during artificial aging.

However, both knockout and overexpression of *OsNAT9* disturbed the homeostasis of AsA pools in the apoplast and symplast, leading to varying degrees of ROS accumulation and diminished seed vigor. Conversely, overexpression of *OsNAT9* increased the AsA concentration in young leaves and improved drought tolerance in rice. In conclusion, our findings demonstrate that *OsNAT9*-mediated AsA efflux is crucial for regulating redox homeostasis in the apoplast and symplast, thereby playing a significant role in seed vigor and stress adaptation in rice.

RESULTS

OsNAT9 encodes a nucleobase–ascorbate transporter

Two rice varieties exhibiting contrasting levels of seed storability, namely, *Oryza sativa* L. *indica* cv. Fuxiangzhan (FXZ), characterized by high storage tolerance, and *O. sativa indica* cv. H603, characterized by low storage tolerance, were identified by screening on the basis of seed storability evaluation tests (Figure S1A). To elucidate the molecular mechanisms underlying the difference in storability between the two rice varieties, a comparative proteomic analysis was performed on the seed embryos between the two varieties after artificial aging for different periods of time. A total of 25 significantly differentially accumulated proteins (DAPs) were found to be markedly regulated after 15 days post-artificial aging (Figure S2). Among these proteins, the accumulation and mRNA transcript abundance of the B8AIE1 protein were reduced more in the low-storability "H603" than in the high-storability "FXZ" during artificial aging (Figure S2). BLAST analysis revealed that the B8AIE1 protein, encoded by *Os03g0694500*, belonged to the *NAT* gene family, subsequently designated as *OsNAT9*. Phylogenetic analysis indicated that NATs could be divided into five clades, I to V, with NAT9 belonging to clade IV and exhibiting high homology with maize LPE1 (Figure S1D). Further analysis of the protein structure indicated that OsNAT9 consists of 10 transmembrane domains, as well as a conserved QH domain and a [Q/E/P]-N-X-G-X_4-T-[R/K/G] domain (Figures S1E,F, S3). Previous structural studies had identified the [Q/E/P]-N-X-G-X_4-T-[R/K/G] domain as a critical signature motif that determines the function of NAT proteins in transporting nucleobases or ascorbate (Wang, He, et al., 2023). Maize LPE1 has been characterized as a transporter of uric acid or xanthine (Argyrou et al., 2001). The NAT signature motif in OsNAT9 showed high sequence identity with that of maize LPE1 (Figure S1F), suggesting that OsNAT9 may perform similar functions.

Expression patterns of *OsNAT9* and subcellular localization of OsNAT9

The expression profiles of *OsNAT9* were investigated across various plant organs. As illustrated in Figure 1A, *OsNAT9* showed significant expression predominantly in the stems, embryos, shoots, and early-stage seedlings, with particular prominence in grains at the milk stage and in 10-day-old seedlings. The expression patterns of *OsNAT9* were evaluated under various treatments. The transcript levels of *OsNAT9* were found to be consistently upregulated within 12 h of exposure to NaCl or H_2O_2, and within 24 h of exposure to PEG6000 (polyethylene glycol 6000), AsA, or jasmonic acid (JA) treatments, subsequently exhibiting a downward trend (Figure 1B–F). In contrast, within 8 h of salicylic acid (SA) or abscisic acid (ABA) treatment, the expression levels of *OsNAT9* showed a gradual upregulation, followed by a slight decline, and then a sharp increase at 36 h post-treatment (Figure 1G–H).

To corroborate the quantitative real-time PCR (qPCR) results, transgenic plants expressing *proOsNAT9::GUS* were generated. Histochemical staining revealed strong GUS activity in grains at the milk stage, followed by the leaf sheath, with weaker activity in early-stage panicles (Figure 1I). During seed germination, GUS activity was predominantly observed in the shoots and roots (Figure 1I). In addition, enhanced GUS activity was observed in response to treatment with NaCl, ABA, SA, H_2O_2, PEG6000, or AsA (Figure 1J), indicating that the expression of *OsNAT9* can be induced by these factors. These findings are consistent with the qPCR results.

To investigate the subcellular localization of OsNAT9, the *proOsUbi::OsNAT9-GFP* construct was introduced into *O. sativa japonica* cv. Tainung 67 (TNG67) using an *Agrobacterium tumefaciens*-mediated transformation system. The fluorescent signal of the OsNAT9-GFP fusion was predominantly observed on the cytomembrane, exhibiting either a uniform or a punctate (dotted) pattern, and co-localizing with the signal from the cell membrane dye FM4-64 (Figure 1K,L). These results indicate that OsNAT9 acts as a cytomembrane-localized nucleobase–ascorbate transporter.

OsNAT9 regulates seed vigor and storability

We designed the CRISPR target site for exon 4 of the *OsNAT9* gene and generated two independent CRISPR knockout mutants, *Osnat9-1* and *Osnat9-2*. Homozygous mutant lines were isolated through PCR-based genotyping. The *Osnat9-1* and *Osnat9-2* mutants exhibited a 1-bp insertion and a 2-bp deletion in the fourth exon, respectively (Figure 2A,B). These mutations lead to premature termination of OsNAT9 translation, suggesting a potential loss of functional OsNAT9 protein in these mutants. For overexpression analysis, transgenic lines exhibiting significantly altered *OsNAT9* expression levels compared with the TNG67 wild-type line were selected for further analysis (Figure 2C,D). To investigate the role of *OsNAT9* in regulating seed vigor, we examined the seed germination processes in wild-type, *Osnat9* mutants, and

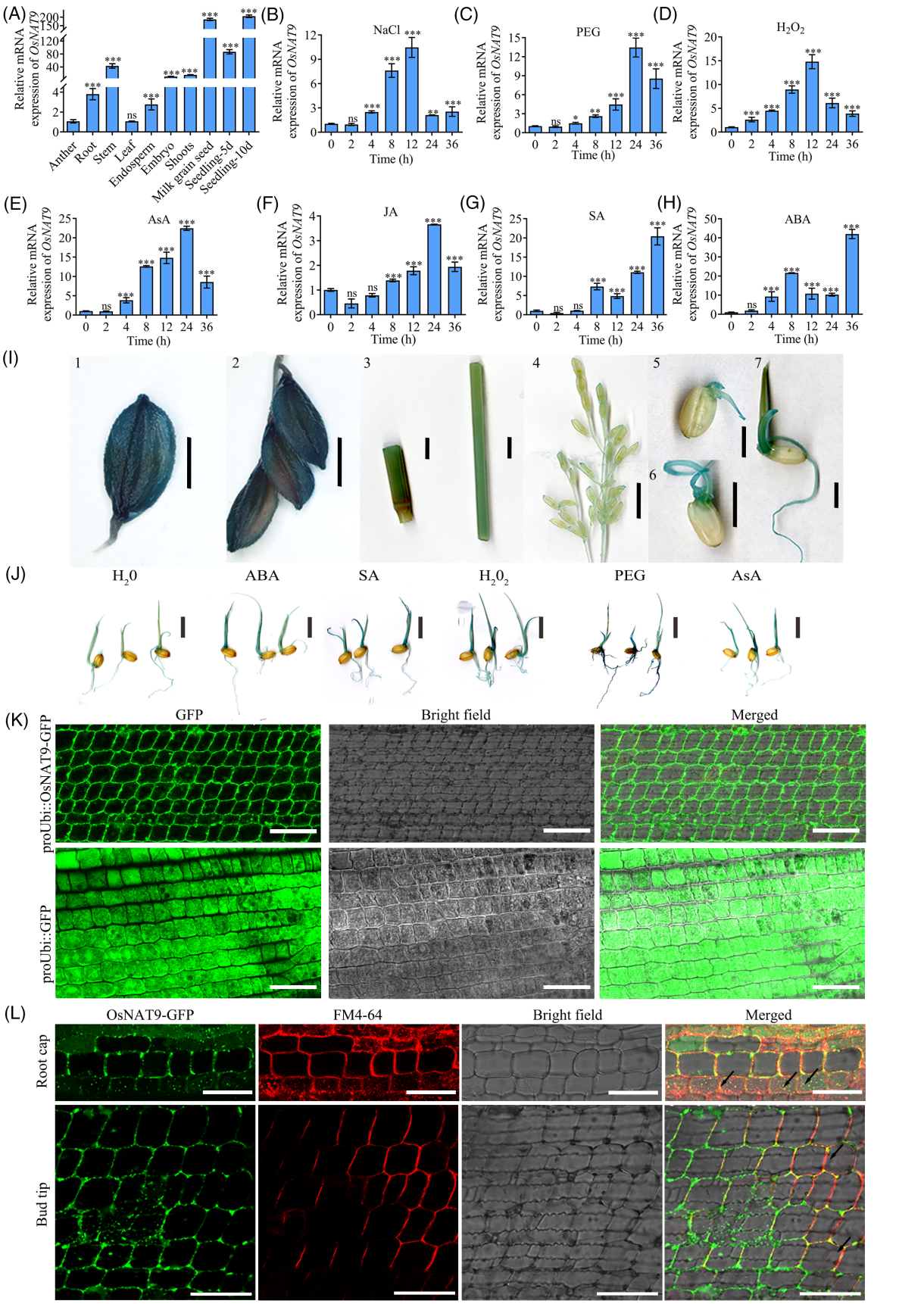

Figure 1. Expression patterns of *OsNAT9* and subcellular localization of OsNAT9.
(A) Quantitative real-time PCR (qPCR) analysis of *OsNAT9* expression in different organs of the wild-type rice, "TNG67."
(B–H) qPCR analysis of the time course of *OsNAT9* expression induced by abiotic stresses. Fourteen-day-old "TNG67" seedlings were treated with 150 mM NaCl (B), 25% polyethylene glycol 6000 (PEG6000) (C), 20 mM hydrogen peroxide (H^2O^2) (D), 100 μM abscisic acid (ABA) (E), 100 μM jasmonic acid (JA) (F), 100 μM salicylic acid (SA) (G), or 15 mM ascorbic acid (AsA) (H), and compared with a distilled water-treated control.
Total RNA was extracted at the times indicated. The data (A–H) are shown as mean ± standard deviation, from three independent replicates. The expression level of *OsNAT9* was monitored using qPCR, with the *OsActin150* gene as control. The relative expression levels are represented as fold-changes relative to the expression level of *OsNAT9* in leaf tissue at 0 h under the H_2O treatment. Asterisks indicate significant differences compared with the untreated control (ns, no significant difference. $*P < 0.05$; $**P < 0.01$, $***P < 0.001$) according to ANOVA and Fisher's LSD.
(I) Histochemical localization of GUS activity in the *proOsNAT9::GUS* transgenic plants at different development stages. Scale bars = 1 cm.
(J) Histochemical localization of GUS activity in the *proOsNAT9::GUS* transgenic plants under different abiotic stresses. Scale bars = 1 cm.
(K) Subcellular localization of *OsNAT9-OE* (overexpression) lines tagged at the C terminus with green fluorescent protein (GFP) in rice roots. Scale bars = 500 μm.
(L) The OsNAT9-GFP co-localized with the signal from the cell membrane dye FM4-64 in rice root cap and bud tip. Scale bars = 500 μm.

OsNAT9-overexpression *(OsNAT9-OE)* lines, calculating the germination potential (GP) at 3 days after 24 h of imbibition, germination rate (GR) at 7 days after 24 h of imbibition, and germination index (GI) in each. Compared with the wild-type, *Osnat9* mutants showed significant decreases in these metrics, whereas the *OsNAT9-OE* lines showed either no significant difference or a trend toward increased values (Figure 2E–H), indicating that *OsNAT9* is required for seed germination. Generally, seed dormancy negatively impacts seed germination. To further investigate the mechanism underlying seed germination inhibition by knocking out *OsNAT9*, seed germination tests were performed after breaking dormancy. Interestingly, GP, GR, and GI in *Osnat9* mutants were significantly improved, although they remained lower than those in the wild-type and the *OsNAT9-OE* lines (Figure S4). These results suggest that seed dormancy may be a primary factor contributing to the inhibition of seed germination in *Osnat9* mutants.

Seed aging is characterized by the irreversible decline in seed vigor and germination ability during storage (Oenel et al., 2017; Solberg et al., 2020; Wang et al., 2018). To investigate the impact of the *OsNAT9* gene on seed storability, the seed vigor of rice of different genotypes (wild-type, *Osnat9* mutants and *OsNAT9-OE* lines of "TNG67") was evaluated under natural and artificial aging conditions. After 6 months of natural storage and aging, the GP, GR, and GI of *OsNAT9-OE* lines were significantly lower than those of the wild-type seed, yet significantly higher than those of the *Osnat9* mutants (Figure S5). After the artificial aging treatment, the GP, GR, and GI of the wild-type, *Osnat9* mutants, and *OsNAT9-OE* lines all exhibited a marked decrease relative to the corresponding unaged seeds (Figure 3A,B). Consistent with the results from natural aging, the GP and GR of the *OsNAT9-OE* lines were significantly lower than those of the wild-type line but exceeded those of the *Osnat9* mutants (Figure 3B). These findings indicate that both the knockout and overexpression of the *OsNAT9* gene adversely affect the storability of rice seeds. During seed germination, the endosperm serves as a critical source of energy and nutrients, facilitating embryo growth and development (Lima et al., 2024). To elucidate the factors influencing seed storability, the endosperm structure of rice seeds of different genotypes was analyzed post-aging. After 14 days of artificial aging, localized regions of chalkiness were observed in the endosperm of both wild-type and *OsNAT9-OE* lines, characterized by a white and opaque appearance (Figure 3C). At the same time, the entire endosperm of *Osnat9-1* mutant seeds exhibited serious chalkiness (Figure 3C). Scanning electron microscopy (SEM) analysis revealed that the starch particles within the endosperm of aged *Osnat9-1* mutant seeds were irregularly round and loosely arranged (Figure 3D), indicating that significant structural damage had occurred to the endosperm due to the aging treatment. Nitroblue tetrazolium (NBT) staining demonstrated a denser distribution of ROS in the endosperm of *Osnat9* mutants than in wild-type and *OsNAT9-OE* lines after both 7 and 14 days of artificial aging (Figure 3E). This indicates that aging induced substantial ROS accumulation in the endosperm of *Osnat9* mutants, thereby compromising the starch granule structure and affecting energy and nutrient supply during seed germination.

Although the degree of endosperm chalkiness in the *OsNAT9-OE* lines was comparable to that in the wild-type line after artificial aging treatment (Figure 3C,D), there was a significant reduction in the seed vigor of the overexpressed lines (Figure 3B). To elucidate the underlying causes of this reduced seed vigor in *OsNAT9-OE* lines, we assessed the vigor of seed embryos after artificial aging. Staining with 2,3,5-triphenyl tetrazolium chloride (TTC) showed that the embryo vigor in both *Osnat9* mutants and *OsNAT9-OE* lines was significantly lower than that in the wild-type line in response to aging (Figure 3F). To further explore the factors contributing to the decreased viability of seed embryos, we measured the concentrations of hydrogen peroxide (H_2O_2) and malondialdehyde (MDA), along with the activities of antioxidant enzymes in the embryos. Our findings demonstrated that the concentrations of H_2O_2 and MDA were elevated in the embryos of

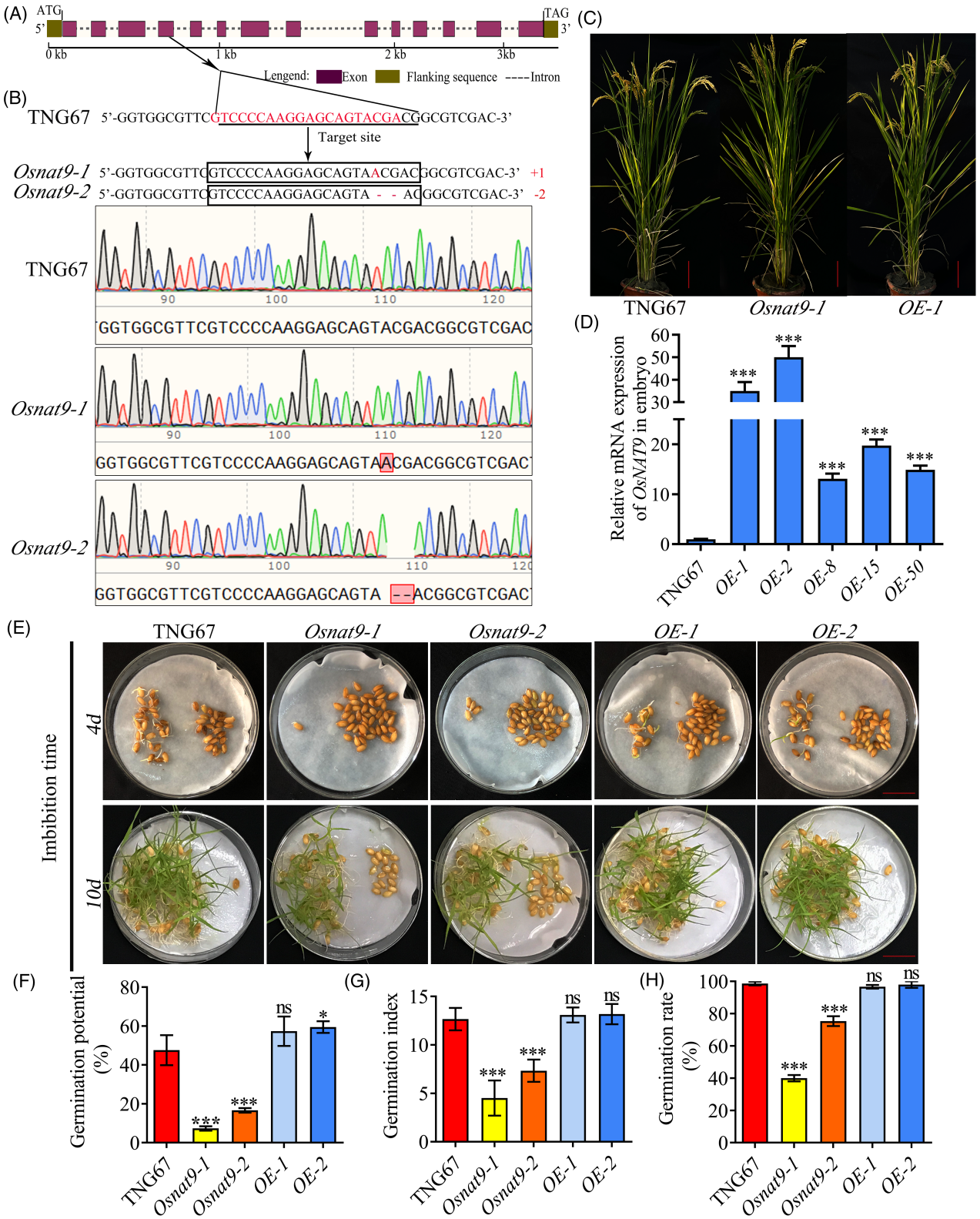

Figure 2. Knockout of OsNAT9 resulted in reducing seed vigor in *Oryza sativa*.
(A) Schematic diagram of the *OsNAT9* genome. CRISPR/Cas9 target sites were designed on the fourth exon.
(B) Base mutation site and sequencing peak map of the mutation site. A 1-base pair (bp) insertion was detected in the *Osnat9-1* mutant, and a 2-bp deletion was detected in the *Osnat9-2* mutant. Target sites are marked in red. The sequences in boxes show the target sequences in cultivar TNG67. Red dashes represent the deleted bases, and inserted bases are indicated by red uppercase letters.
(C) Photographs of plants of "TNG67" wild-type, the *OsNAT9* mutants, and *OsNAT9* overexpressed (*OsNAT9-OE*) lines, Scale bar = 10 cm.
(D) Relative expression analysis of the *OsNAT9* gene in wild-type "TNG67" and *OsNAT9-OE* lines.
(E) Photographs of germinated seeds of wild-type "TNG67," the *Osnat9* mutants, and *OsNAT9-OE* lines at 4 and 10 days after germination, Scale bar = 2 cm.
(F–H) The germination potential (GP) at 3 days after 24 h of imbibition (F), germination rates (GR) at 7 days after 24 h of imbibition (G), and germination index (GI) (H) of wild-type "TNG67," the *Osnat9* mutants, and *OsNAT9-OE* lines. Each column represents the mean ± standard deviation of three biological replicates. ns, no significant difference. $*P < 0.05$ and $***P < 0.001$, compared with the wild-type "TNG67" control; ns means not significant, using ANOVA and Fisher's LSD.

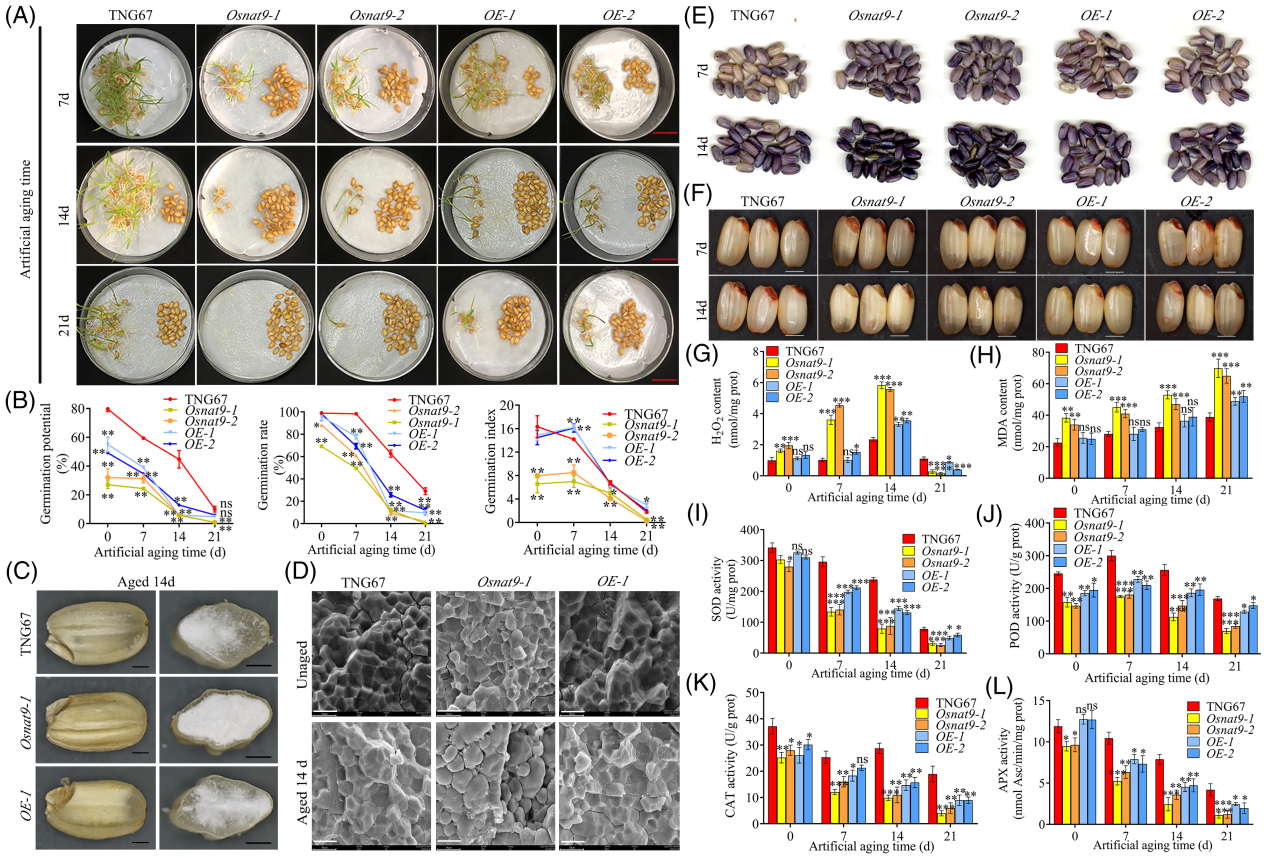

Figure 3. Comparison of rice seed vigor among wild-type "TNG67," *Osnat9* mutants, and *OsNAT9* overexpression lines after artificial aging.
(A) Photographs of germinated seeds of "TNG67," *Osnat9* mutants, and *OsNAT9-OE* lines at 7 days post-imbibition after artificial aging for 7, 14, or 21 days. Scale bar = 2 cm.
(B) Comparison of GP, GR, and GI of the wild-type "TNG67," *Osnat9* mutants, and *OsNAT9-OE* lines after different durations of artificial aging. Age-matched seeds were used for all germination experiments ($n = 50$ per replicate). In the linear charts, the values represent the mean ± standard deviation of three biological replicates. $*P < 0.05$, $**P < 0.01$, and $***P < 0.001$, compared with the "TNG67" control, using ANOVA and Fisher's LSD.
(C) Rice grain appearance of the "TNG67," *Osnat9* mutants, and *OsNAT9-OE* lines after artificial aging for 14 days. Scale bar = 100 μm.
(D) Scanning electron microscopy images of rice grain cross-sections of the "TNG67," *Osnat9* mutants, and *OsNAT9-OE* lines after artificial aging for 14 d. Scale bar = 10 μm.
(E) Tetrazolium assay for seed viability and (F) NBT staining for H_2O_2 production of the wild-type "TNG67," *Osnat9* mutants, and *OsNAT9-OE* lines after 7 and 14 days of artificial aging.
(G–L) The H_2O_2 concentration (G), malondialdehyde (MDA) concentration (H), superoxide dismutase (SOD) activity (I), peroxidase (POD) activity (J), catalase (CAT) activity (K), and ascorbate peroxidase activity (APX) (L) in the seeds of the "TGN67," the *Osnat9* mutants, and *OsNAT9-OE* lines. In the bar charts, the values represent the mean ± standard deviation of three biological replicates. ns, no significant difference. $*P < 0.05$, $**P < 0.01$, and $***P < 0.001$, compared with the wild-type "TNG67" control, using ANOVA and Fisher's LSD.

the *Osnat9* mutant relative to the wild-type line (Figure 3G–H). Similarly, both concentrations were higher in the *OsNAT9-OE* lines than in the wild-type line at both 14 and 21 days of artificial aging (Figure 3G–H). Furthermore, the activities of antioxidative enzymes, including superoxide dismutase (SOD), peroxidase (POD), catalase (CAT), and ascorbate peroxidase (APX), were significantly lower in both the *Osnat9* mutant and *OsNAT9-OE* lines than in the wild-type line during artificial aging (Figure 3I–L). These results suggest that artificial aging induces substantial ROS accumulation in the embryos of *Osnat9* mutants and *OsNAT9-OE* lines, thereby impairing embryo vigor and consequently inhibiting seed germination.

Metabolomic analysis identifies key metabolites regulated by *OsNAT9* in seed aging

To investigate the influence of *OsNAT9* on changes in the concentrations of metabolites in rice seeds during the aging process, we conducted a comparative metabolic analysis between seed embryos in the wild-type and *Osnat9* mutants (*Osnat9-1* and *Osnat9-2*) at 0, 7, and 14 days of artificial aging. A total of 1093 differentially accumulated metabolites (DAMs) were identified, which were primarily categorized into nine classes, namely flavonoids, lipids, phenolic acids, alkaloids, amino acids and derivatives, nucleotides and derivatives, organic acids, lignans and coumarins, and terpenoids (Figure 4A). Among them, flavonoids, lipids, and phenolic acids accounted for 22.14%, 14.46%, and 14.18% of the total DAMs, respectively (Figure 4A). In a comparative study between the wild-type line and the *Osnat9-1* mutant, 196 DAMs were identified prior to aging, 293 DAMs were observed after 7 days of artificial aging, and 187 DAMs were noted after 14 days of artificial aging (Figure 4B). Similarly, in the comparison between the wild-type and the *Osnat9-2* mutant, 252 DAMs were detected before aging, 255 DAMs were identified after 7 days of artificial aging, and 241 DAMs were found after 14 days of artificial aging (Figure 4B). A comparative analysis across these three time points revealed that 47 DAMs consistently differed significantly between the wild-type line and the *Osnat9-1* mutant, while 46 DAMs persisted between the wild-type line and the *Osnat9-2* mutant (Figure 4C). This indicates that the concentrations of these metabolites underwent sustained changes during the aging process as affected by the *OsNAT9* gene. The Kyoto Encyclopedia of Genes and Genomes (KEGG) pathway enrichment analysis revealed a significant enrichment of flavonoid biosynthesis, glutathione metabolism, ascorbate and aldarate metabolism, as well as galactose metabolism, among the DAMs between the wild-type line and the *Osnat9* mutants at both 7 and 14 days of artificial aging (Figure 4D,E; Figure S6). The concentrations of metabolites involved in these pathways exhibited significant variations between the wild-type line and the *Osnat9* mutants (Figure 4F–H), suggesting potential impacts on the cellular redox state during the aging process. AsA and glutathione are critical antioxidant compounds within cells, with their metabolic processes intricately linked to the cellular redox state (Pignocchi & Foyer, 2003). In addition, the *de novo* biosynthesis of AsA relies on galactose metabolism, whereas the recycling pathway of AsA is dependent on the glutathione metabolic cycle (Pignocchi & Foyer, 2003). It is hypothesized that OsNAT9, functioning as an ascorbate-nucleoside transporter, may influence the antioxidant capacity of seeds during aging by modulating the metabolism of AsA and glutathione.

***OsNAT9* regulates seed vigor through influencing AsA concentration**

To examine the influence of *OsNAT9* on AsA accumulation, we measured the AsA concentration in various rice organs, including seeds, embryos, endosperms, stems, and leaves, across different genotypes. Compared with other organs, AsA accumulation was significantly higher in embryos and leaves (Figure 5A). Furthermore, no significant difference in AsA concentration was observed between *OsNAT9-OE* lines and wild-type, although the AsA concentration in *Osnat9* mutants was markedly lower than in the wild-type line (Figure 5A). During the artificial aging process, AsA concentration in the embryos of the wild-type, *Osnat9* mutants, and *OsNAT9-OE* lines increased in the early stages but gradually decreased during the later stages (Figure 5B). Interestingly, AsA concentration in the embryos of *Osnat9* mutants was significantly higher than that in the wild-type after 7 days of artificial aging, whereas the concentration in the *OsNAT9-OE* lines was significantly lower than in the wild-type (Figure 5B). By 14 days of artificial aging, AsA concentrations in the embryos of both *Osnat9* mutants and the *OsNAT9-OE* line were significantly lower than in the wild-type (Figure 5B). To further investigate the source of AsA biosynthesis in rice seed embryos during aging, gene expression analysis in seed embryos was conducted during the aging process. Prior to aging, the expression levels of genes associated with the *de novo* biosynthesis and recycling pathways of AsA in *Osnat9* mutant embryos were significantly higher than those in the wild-type, whereas the expression level of the aldanolactonase gene (*Os05g0474600*) was markedly lower (Figure 5C–J). Conversely, in *OsNAT9-OE* lines, the expression levels of these genes involved in the AsA de novo biosynthesis and recycling pathway were significantly lower than in the wild-type line, except for the *OsMDHAR1* gene (*Os08g0151800*), which showed no significant difference in expression among the lines (Figure 5C–J). However, after 14 days of artificial aging, the expression levels of genes related to the AsA *de novo* biosynthesis pathway in

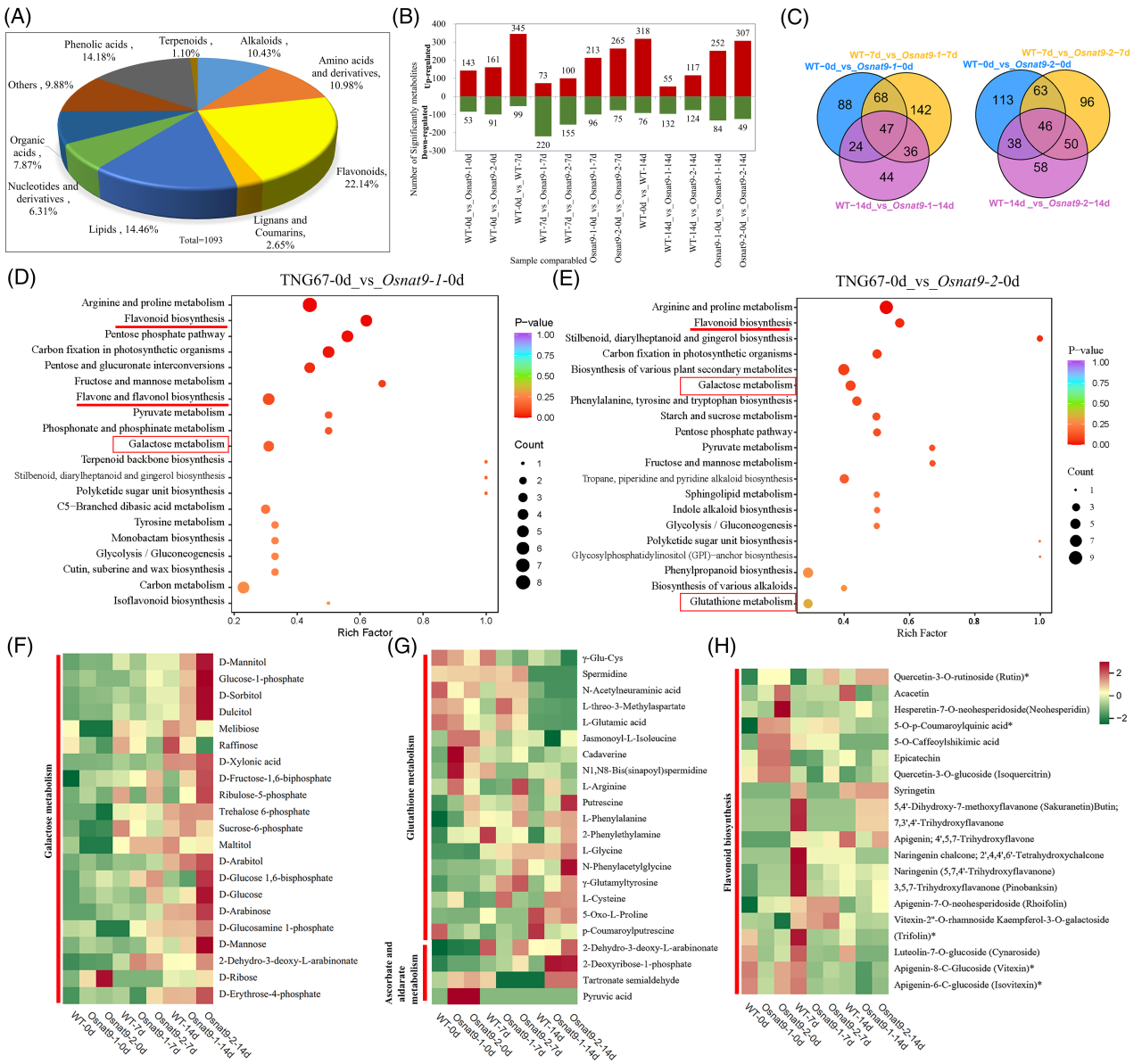

Figure 4. Metabolomic analysis of seed embryos of wild-type "TGN67" and *Osnat9* knockout mutants during artificial aging.
(A) Classification of metabolites.
(B) Up- and down-regulated metabolites detected between "TGN67" and *Osnat9* mutants.
(C) Venn diagram of the differentially accumulated metabolites (DAMs) between "TGN67" and *Osnat9* mutants.
(D–E) KEGG enrichment analysis of the DAMs between "TGN67" and *Osnat9* mutants.
(F–H) DAMs of galactose metabolism, glutathione metabolism, ascorbate and aldarate metabolism, and flavonoid biosynthesis between "TGN67" and *Osnat9* mutants.

both *Osnat9* mutants and *OsNAT9-OE* lines were significantly lower than those in the wild-type parent line (Figure 5C–F). In contrast, the expression levels of genes related to the ASA recycling pathway were significantly higher in *Osnat9* mutants and *OsNAT9-OE* lines than in the wild-type line (Figure 5G–J). These findings suggest that AsA is primarily derived from the *de novo* biosynthesis pathway in wild-type seed embryos during the aging process, whereas, in contrast, the AsA source predominantly relies on the recycling pathway in *Osnat9* mutants and *OsNAT9-OE* lines. To investigate whether the *OsNAT9* gene regulates rice seed vigor by modulating AsA concentrations, the germination capacity of rice seeds was assessed in medium containing different concentrations of AsA. The results demonstrated that treatment with 0.3 mM exogenous AsA significantly restored the GP, GR,

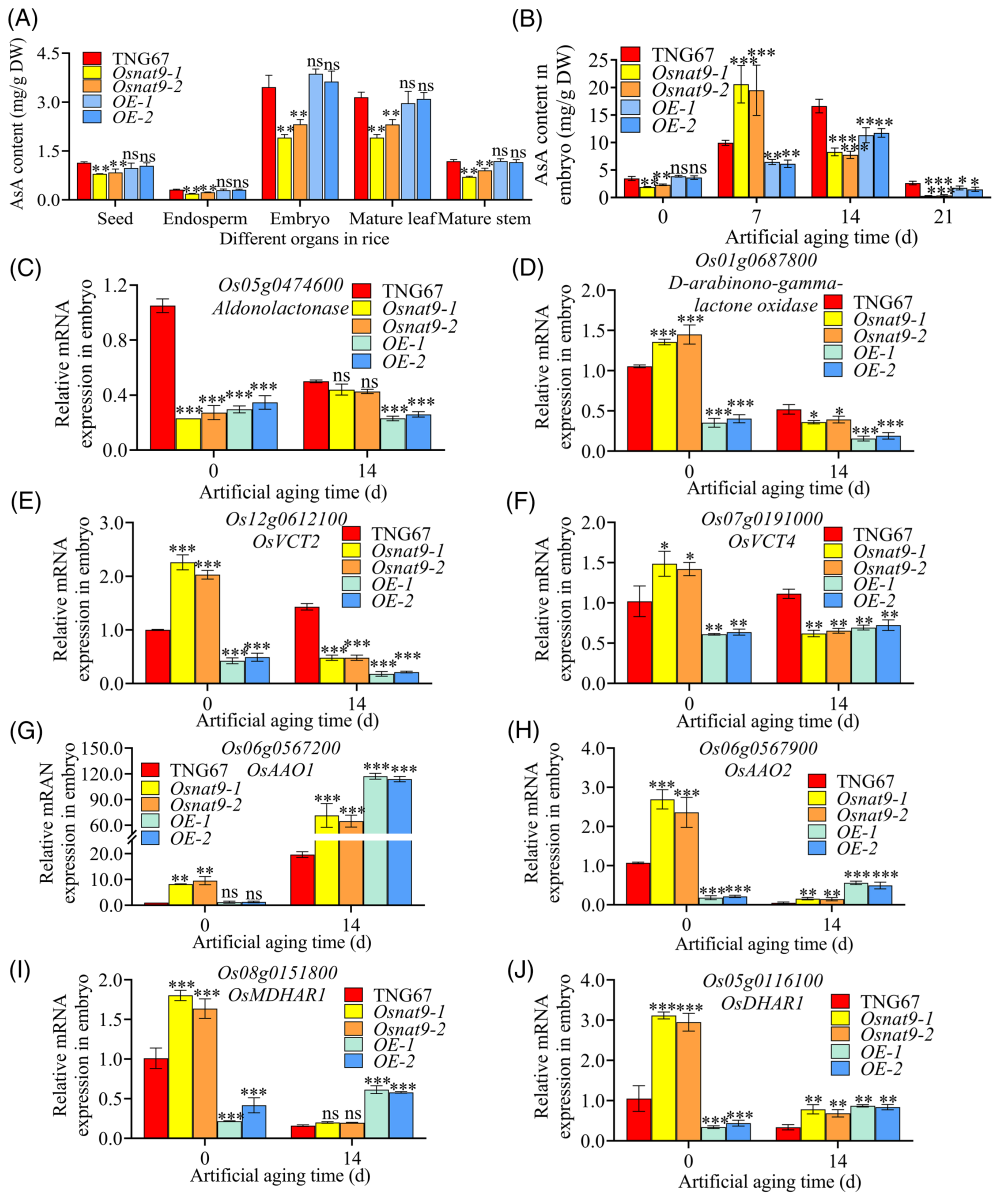

Figure 5. *OsNAT9* knockout induced an imbalance of AsA levels and changes in the mRNA abundance from the AsA biosynthesis and recycling genes during artificial aging.
(A) The AsA concentration in the different organs of wild-type "TGN67," *Osnat9* mutants, and *OsNAT9-OE* rice. The seeds, embryo, endosperm, old leaves, and old stems were harvested from mature stage rice materials grown in the field.
(B–C) AsA concentration in the embryo and endosperm of "TGN67," the *Osnat9* mutants, and *OsNAT9-OE* lines during artificial aging (0–21 days).
(C–J) Expression of the genes involved in the AsA biosynthetic and recycling pathways in the embryos of wild-type "TGN67," the *Osnat9* mutants, and the *OsNAT9-OE* lines during artificial aging. In the bar charts, the values represent the mean ± standard deviation. ns, no significant difference, $*P < 0.05$, $**P < 0.01$ and $***P < 0.001$, compared with the "TGN67" control by ANOVA and Fisher's LSD.

and GI parameters of the *Osnat9* mutants to levels comparable to those of the wild-type line (Figure S7). However, as the concentration of exogenous AsA increased, the SP, GP, and GI of the *Osnat9* mutants progressively declined (Figure S7). It is hypothesized that this decline might be attributed to the inability of the *Osnat9* mutants to effectively maintain AsA homeostasis *in vivo*, leading to reduced seed germination capacity.

OsNAT9 confers drought tolerance through increasing AsA concentration in rice

AsA is crucial for plant adaptation to various stresses (Pignocchi & Foyer, 2003). Our study demonstrated that knockout of the *OsNAT9* gene significantly decreased AsA levels in rice (Figure 5A). This observation led us to hypothesize that the *OsNAT9* gene is involved in

regulating not only seed vigor but also response to other stresses. The expression levels of the *OsNAT9* gene were upregulated by PEG and ABA (Figure 1C,H), suggesting its potential regulatory role in rice drought tolerance. To evaluate this hypothesis, we employed a 25% (w/v) PEG solution to simulate drought stress in different accessions of cultivated rice. After 21 days of PEG treatment, both wild-type and *Osnat9* mutant plants exhibited severe wilting, with the wilted *Osnat9* mutants phenotype being particularly pronounced, whereas the *OsNAT9-OE* lines displayed enhanced drought tolerance (Figure 6A). Following a 7-day recovery period after 21-day exposure to PEG, the survival rate of *Osnat9* mutant plants was significantly lower than that of the wild-type, whereas the *OsNAT9-OE* lines exhibited a significantly higher survival rate compared with the wild-type line (Figure 6B), further confirming the positive role of the *OsNAT9* gene in drought tolerance. To examine the accumulation of ROS under drought stress, we conducted 3,3′-diaminobenzidine (DAB) and NBT staining on rice leaves. The results revealed that the distribution density of ROS was greater in mutant leaves than in the wild-type or *OsNAT9-OE* leaves (Figure 6C,D). Subsequent analyses demonstrated that, in response to drought exposure, the levels of H_2O_2 and MDA in *Osnat9* leaves were significantly higher than those in the wild-type and the *OsNAT9-OE* lines (Figure 6E,F), indicating that drought stress resulted in substantial ROS accumulation in mutant *Osnat9* leaves. To elucidate the underlying mechanism of ROS accumulation in mutant leaves under drought stress, we assessed the activity of antioxidant enzymes and the AsA concentration in the leaves. The results showed that the activities of CAT, POD, and SOD were significantly reduced in the *Osnat9* mutants compared with the wild-type and *OsNAT9-OE* lines under drought stress (Figure 6G–I), indicating that the knockout of the *OsNAT9* gene impairs antioxidant enzyme activity in rice leaves. In addition, the AsA concentration decreased significantly across all rice genotypes in response to drought stress (Figure 6J). However, under both normal and drought conditions, the AsA concentrations in *Osnat9* mutants were significantly lower than in the wild-type, whereas they were significantly higher in *OsNAT9-OE* lines compared with the wild-type line (Figure 6J). These results suggest that the *OsNAT9* gene may enhance drought tolerance in rice by increasing the AsA concentration in leaves. Additionally, our study reveals that flag leaves exhibit significantly higher expression levels of genes associated with both de novo AsA biosynthesis and recycling pathways compared with older leaves (Figure S8). This indicates a more robust AsA biosynthesis capacity in young leaves. In conclusion, the *OsNAT9* gene plays a significant role in rice response to drought stress through the regulation of AsA concentration and antioxidant enzyme activity.

OsNAT9 is an efflux transporter responsible for AsA secretion

OsNAT9 belongs to the *NAT* gene family, and alterations in the expression of the *OsNAT9* gene, either through knockout or overexpression, can modify the AsA concentration in plants (Figure 5A,B). Based on these observations, we speculated that *OsNAT9* may be involved in the AsA transport process. To evaluate the impact of *OsNAT9* on AsA transport, we employed a protoplast secretion assay. The protoplasts were isolated from *OsNAT9-OE* lines, *Osnat9* mutants, and wild-type rice plants, and subsequently cultured with varying concentrations of dehydroascorbic acid (DHA), a precursor in the AsA recycling pathway, to measure changes in AsA concentration within the protoplasts and the surrounding culture medium. The findings indicated that the AsA concentration in the medium of the *Osnat9* mutant protoplasts was significantly lower than that of the wild-type protoplasts upon the addition of DHA at varying concentrations (Figure 7A). Conversely, the AsA concentration in the medium of *OsNAT9-OE* protoplasts was significantly higher than that of the wild-type protoplasts (Figure 7A). Furthermore, the AsA concentration within the *Osnat9* mutant protoplasts was significantly higher than that in the wild-type protoplasts, whereas the AsA concentration in the protoplasts of *OsNAT9-OE* lines was significantly lower than that in the wild-type protoplasts (Figure 7B). These results imply that *OsNAT9* plays a role in regulating the cellular secretion of AsA. Specifically, the loss of *OsNAT9* function in the knockout mutants led to an intracellular accumulation of AsA, accompanied by diminished secretion into the culture medium. In *OsNAT9-OE* protoplasts, elevated *OsNAT9* expression facilitated the secretion of AsA into the culture medium and reduced intracellular AsA levels.

To further investigate whether AsA is a targeted substrate for transport by the OsNAT9 protein, we employed the microscale thermophoresis technique (MST) to assess the binding interaction between the OsNAT9 protein and AsA. The results indicated that the fluorescence signal of the control green fluorescent protein (GFP) remained largely unchanged in response to different concentrations of AsA (Figure 7C), suggesting that GFP did not interact with AsA. In contrast, the fluorescence signal of OsNAT9-GFP exhibited a significant dose-dependent change in response to increasing AsA concentration, eventually reaching saturation (Figure 7C). These results suggest a strong binding affinity between the OsNAT9 protein and AsA. Further analysis revealed that the dissociation constant (K_d) for the GFP control protein in complex with AsA was 2.54 ± 0.65 nM, whereas the K_d for the OsNAT9-GFP protein was 0.12 ± 0.72 nM (Figure 7C), confirming the high-affinity interaction between the OsNAT9 protein and AsA. The substrate-binding capability of the NAT protein

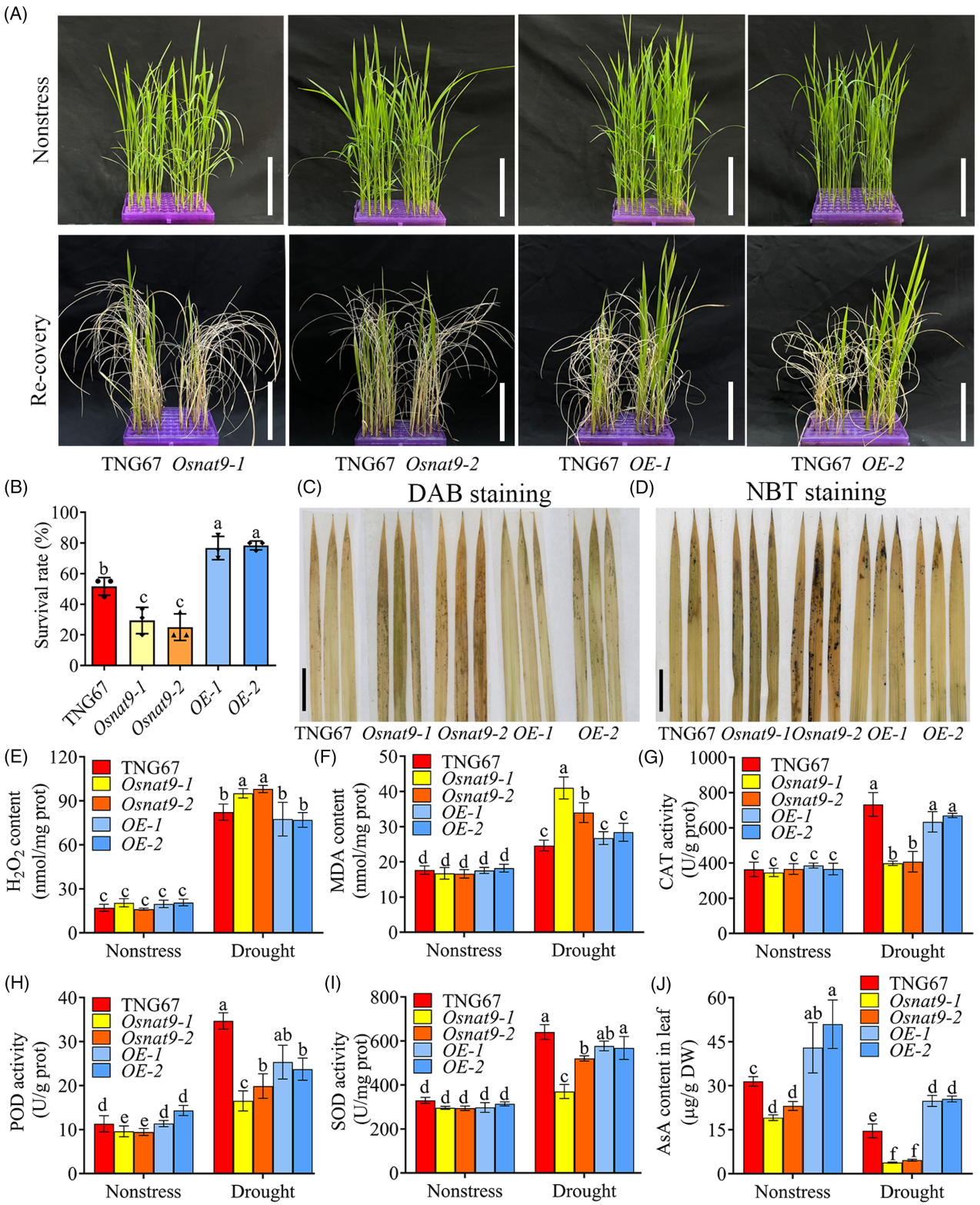

Figure 6. Evaluation of drought tolerance of the "TNG67," *Osnat9* mutants, and *OsNAT9* overexpression lines seedling.
(A) Phenotypic characterization of *Osnat9* mutants, *OsNAT9-OE* lines, and wild-type "TGN67" seedlings under 25% (w/v) PEG6000 treatment. Scale bars = 10 cm.
(B) Survival rates of the knockout, overexpressed lines, and "TGN67" under 25% PEG treatment.
(C–D) DAB and NBT staining of the *Osnat9* mutants, *OsNAT9-OE* lines, and wild-type "TGN67" after 25% PEG treatment for 3 days. Different lowercase letters above the bars indicate significant differences ($P < 0.05$) following ANOVA and Fisher's LSD multiple comparison test. Significant differences were determined using Student's *t*-test.
(E–J) The activities of SOD, POD, CAT, and the concentrations of H_2O_2, MDA, and AsA in the leaves of "TGN67," the *Osnat9* mutants, and *OsNAT9-OE* lines.

family is determined by the NAT signature motif (Kosti et al., 2012). To elucidate the significance of this motif in the binding capacity of the OsNAT9 protein to AsA, site-directed mutagenesis was performed, resulting in the generation of three mutant proteins, namely, $OsNAT9^{S344A}$, $OsNAT9^{E346A}$, and $OsNAT9^{G349A}$. MST analysis revealed that the wild-type GFP-OsNAT9 protein exhibited the highest affinity for AsA ($K_d = 0.28 \pm 0.23$ nM), followed by the $OsNAT9^{G349A}$ mutant protein, which demonstrated a slightly reduced binding affinity ($K_d = 0.55 \pm 0.53$ nM) (Figure 7D). In contrast, the $OsNAT9^{S344A}$ and $OsNAT9^{E346A}$ mutant proteins exhibited a markedly diminished binding affinity for AsA, with K_d values increasing to 100.6 ± 27.56 nM and 80.70 ± 6.06 nM, respectively (Figure 7D). These results suggest that the amino acid residues S^{344} and E^{346} are crucial for the binding capability of the OsNAT9 protein to AsA. Given that LPE1, the maize homolog of OsNAT9, is capable of binding both AsA and xanthine (Argyrou et al., 2001), we hypothesized that xanthine might also serve as a binding substrate for OsNAT9. Subsequent comparative analysis of the binding affinity of OsNAT9 with AsA and xanthine revealed that while OsNAT9 was capable of binding xanthine with a K_d value of 0.39 ± 0.11 nM, its affinity for AsA ($K_d = 0.28 \pm 0.23$ nM) was markedly higher (Figure 7E). In summary, OsNAT9 functions as an efflux protein that specifically binds and exports AsA from the cell, with amino acid residues S^{344} and E^{346} being crucial for this binding interaction.

DISCUSSION

OsNAT9 is a cytomembrane-localized AsA efflux transporter

The regulation of the homeostasis of AsA pools across various cellular compartments, including the apoplast, is mediated by specific ascorbic acid transporters (Horemans et al., 2000; Pignocchi & Foyer, 2003). To date, the known plant AsA transporters include the vacuole-localized TDX5 and the chloroplast-localized PHT4;4 (Hoang et al., 2021; Miyaji et al., 2015), while the identity of cytomembrane-localized AsA transporters remains uncertain. In mammals, the *NAT* gene family members *SVCT1* and *SVCT2* are recognized for their role in AsA transport (Wang, He, et al., 2023). However, the involvement of plant *NAT* gene family members in AsA transport has been little reported. The OsNAT9 protein contains 10 conserved transmembrane domains (Figures S1E and S3) and is predominantly localized on the cytomembrane, either uniformly or in a punctate distribution (Figure 1K,L), suggesting its function as a cytomembrane-localized ascorbate–nucleoside transporter. Within the NAT protein family, the NAT signature motif is associated with the substrate specificity and transport functionality of NAT proteins (Kosti et al., 2012). Compared with the mammalian ascorbate transporters, the NAT motif sequences in the OsNAT9 protein show high homology with the mammalian nucleoside transporters (Figure S1F). The maize LPE1, a homolog of OsNAT9, has been shown to bind both xanthine and AsA (Argyrou et al., 2001). However, the functional expression of *LPE1* in the filamentous fungus *A. nidulans* revealed that LPE1 did not affect the uptake of AsA in the fungus (Argyrou et al., 2001). Our MST experimental data indicated that the OsNAT9 protein exhibited a high affinity for both xanthine and AsA (Figure 7C,E). After preloading with DHA, the expression of *OsNAT9* in protoplasts displayed a significant positive correlation with the concentration of AsA released into the medium (Figure 7A), indicating that OsNAT9 may function as an ascorbic acid efflux transporter. Structural analyses of mammalian ascorbic acid transporters have identified S^{389} and P^{391} as key amino acid residues that distinguish ascorbic acid transporters from other nucleoside transporters (Wang, He, et al., 2023). Notably, the rice NAT9 and maize LPE1 proteins lack the conserved P^{391} residue (Figure S1F), suggesting that the functional differentiation of the NAT protein family in plants may differ from that in mammals. In conclusion, the NAT9 protein is likely to function as an ascorbate efflux transporter localized on the cytomembrane.

OsNAT9 regulates seed germination by modulating seed dormancy

Seed dormancy is a pivotal factor affecting seed germination (Bewley, 1997). Abscisic acid and gibberellins (GAs) play an antagonistic role in the regulation of seed dormancy (Koornneef et al., 1982). ABA induces the cessation of cell division in embryo cells, thus initiating and maintaining seed dormancy (Liu et al., 1994; Wang et al., 1998).

In contrast, GAs counteract the effects of ABA, facilitating seed germination (Debeaujon & Koornneef, 2000). AsA can relieve seed dormancy by modulating the balance of endogenous hormones within seeds. Treatment with exogenous AsA has been demonstrated to enhance cell division and increase the GR of pear seeds (Niu et al., 2024). Further research has shown that AsA reduces ABA levels while increasing GA levels in seeds, thereby decreasing the ABA/GA ratio, relieving seed dormancy, and promoting germination (Niu et al., 2024). In the current study, the AsA

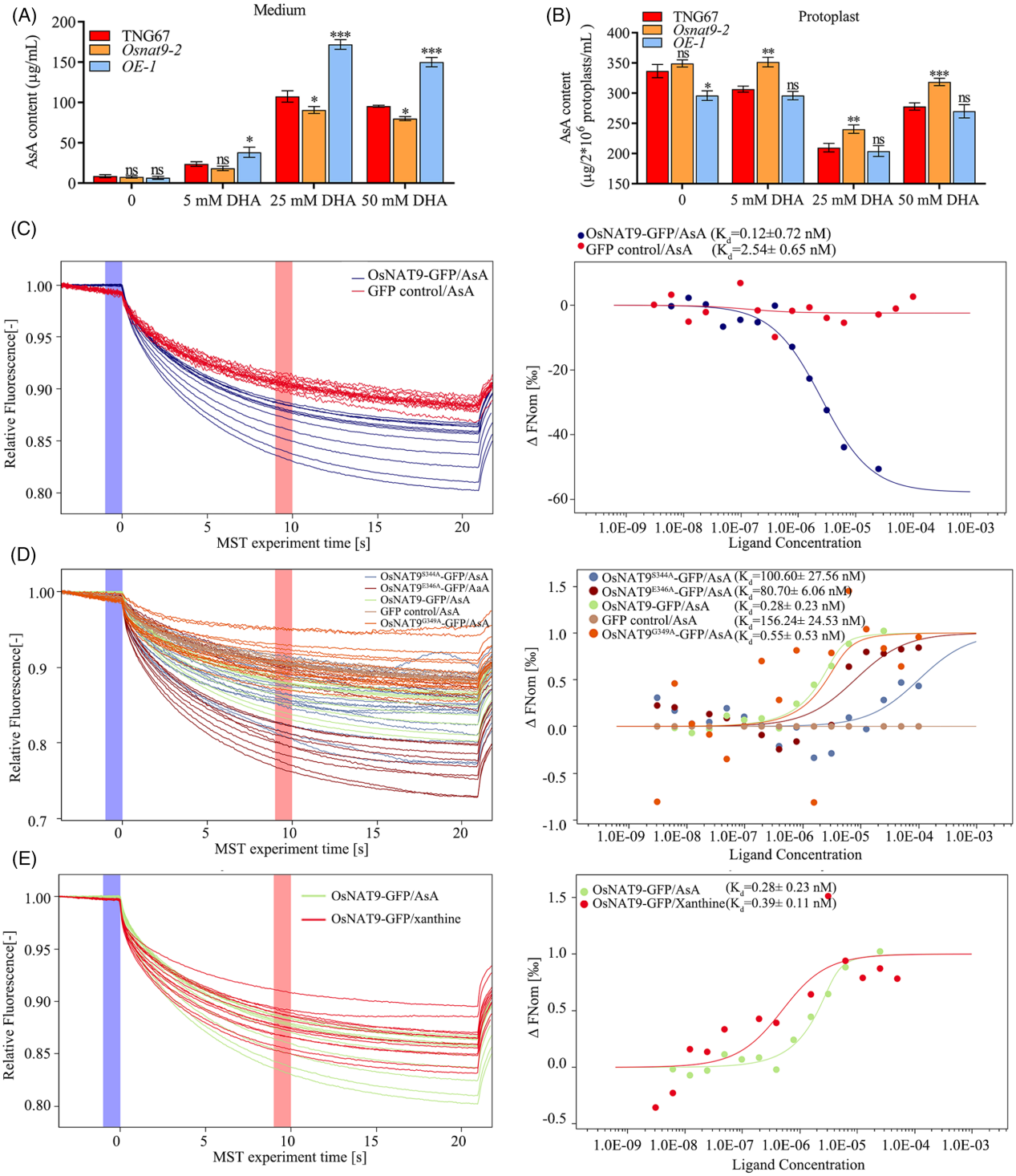

Figure 7. Functional transport expression by OsNAT9 as determined by protoplast secretion and MST assays.
(A, B) Protoplasts isolated from seedlings of wild-type "TGN67," *OsNAT9* mutants, and *OsNAT9-OE* lines were suspended in W5 solution and treated with different concentrations of DHA solution. After overnight incubation for 16 h, the AsA concentrations in W5 solution and protoplasts were determined. Data were expressed as the mean ± standard deviation (n = 3). ns, no significant difference. *P < 0.05, **P < 0.01 and ***P < 0.001, compared with the "TGN67" control by ANOVA and Fisher's LSD.
(C) MST assays for the binding of cGFP-tagged OsNAT9 (OsNAT9-GFP) and AsA *in vitro*.
(D) MST assays were used to detect the binding affinity of the mutants OsNAT9^{S344A}-GFP, OsNAT9^{E346A}-GFP, OsNAT9^{G349A}-GFP, and wild-type OsNAT9-GFP to AsA. Binding curves and K_d values are also shown.
(E) MST assays for the binding of OsNAT9-GFP to AsA or xanthine. Protein and substrate mixtures were loaded into Monolith NT.115 capillaries, and binding was measured using 50% IR laser power and an LED excitation source with λ = 470 nm at ambient temperature.

concentration in the embryo and endosperm of the *Osnat9* mutant was significantly lower than in either wild-type or *OsNAT9-OE* lines (Figure 5A), indicating that the loss of function of *OsNAT9* substantially inhibits AsA accumulation during seed development. Interestingly, the GR of the *Osnat9* mutants was significantly lower under normal conditions (Figure 2G). However, after the seed dormancy was broken, the GR in *Osnat9* mutants was significantly restored (Figure S4). In addition, the application of exogenous AsA also rescued the GR of the *Osnat9* mutants (Figure S7). These results suggested that the reduced AsA concentration in seeds may hinder the ability of the *Osnat9* mutant to break seed dormancy, thereby inhibiting seed germination. Nonetheless, whether the reduced ASA concentration affects seed germination in *Osnat9* mutant by modulating hormone ratios during rice seed germination requires further investigation.

OsNAT9 regulates seed storability by affecting the ROS scavenging system

During the development and subsequent storage of rice seeds, aberrant metabolic processes lead to a disorganized arrangement of starch and protein particles within the endosperm, altering its light transmission properties and resulting in the formation of white opaque regions, known as endosperm chalkiness (He et al., 2024; Wu et al., 2022). This endosperm chalkiness seriously affects the energy and nutrient supply for the development of the embryo during seed germination, thereby reducing both the GR and seedling growth vigor (Fitzgerald et al., 2009). AsA accumulation is crucial for the mitigation of endosperm chalking triggered by seed aging. We found that the AsA concentration in *Osnat9* mutants significantly decreased compared with the wild-type line, whereas *OsNAT9-OE* lines showed no significant difference from the wild-type in terms of AsA concentration (Figure 5A), indicating that the knockout of the *OsNAT9* gene impairs AsA accumulation in seeds. Moreover, the reduced AsA concentration in *Osnat9* mutants increased ROS accumulation in the endosperm, causing severe endosperm chalkiness and inhibiting seed germination and seedling growth (Figure 3A–E). These findings imply that OsNAT9, as a cytomembrane-localized AsA efflux transporter, regulates the viability and stress adaptation of rice seeds by modulating AsA transport and accumulation.

Interestingly, despite the similarities in the ROS concentration and the degree of chalkiness in the aged endosperm of *OsNAT9-OE* lines with those of the wild-type seeds (Figure 3C–E), the seed vigor of *OsNAT9-OE* lines was notably lower than that of the wild-type after aging. This discrepancy may be attributed to an imbalance in the homeostasis of AsA pools between the intracellular and extracellular environments. Within the AsA recycling pathway, intracellular AsA is secreted into the apoplast to mitigate ROS and is subsequently converted to DHA (Horemans et al., 2000; Pignocchi & Foyer, 2003). Given the absence of NADPH and other essential substances for reduction in the apoplast, DHA must be absorbed into the cell via a specific transporter for the reduction and regeneration of AsA (Horemans et al., 2000, Pignocchi & Foyer, 2003). Serving as an efflux transporter of AsA, OsNAT9 may play a critical role in this mechanism. During the initial stages of aging, the AsA concentration in the embryo of the *Osnat9* mutants increased significantly (Figure 5B), potentially due to the augmented AsA biosynthesis triggered by stress signals. However, the AsA efflux mechanism is impaired in the mutants, resulting in the accumulation of AsA within the cell and hindering its secretion and the elimination of ROS in the apoplast. Conversely, the excessive efflux of AsA in the embryos of *OsNAT9-OE* lines results in an accumulation of intracellular ROS due to the lower intracellular AsA concentration, ultimately causing oxidative stress damage to the seed embryos (Figures 3G–H, 5B). Subsequent investigations revealed a marked decline of embryo vigor in both the *Osnat9* mutants and the *OsNAT9-OE* lines during aging, which was accompanied by a significant increase in H_2O_2 and MDA levels, as well as a reduction in antioxidant enzyme activity (Figure 3G,H). These findings confirm that the knockout or overexpression of *OsNAT9* disrupts the homeostasis of AsA pools between intracellular and extracellular environments, resulting in diminished ROS scavenging capacity, damaging embryo development and seed vigor. qPCR analysis indicated that AsA in the wild-type embryo predominantly originates from the *de novo* biosynthesis pathway (Figure 5C–J). In contrast, *Osnat9*

mutant and *OsNAT9-OE* lines exhibited a greater reliance on the recycling pathway (Figure 5C–J), potentially due to a metabolic compensatory mechanism triggered by impaired AsA efflux function. However, this compensatory mechanism was insufficient to fully restore AsA homeostasis, particularly during the later stages of aging. The AsA concentrations in both the *Osant9* mutants and *OsNAT9-OE* lines were significantly lower than that observed in the wild-type line, exacerbating ROS accumulation and cellular damage (Figures 3G,H, 5B). In conclusion, OsNAT9 regulates the homeostasis of the AsA pools by facilitating AsA efflux, thereby maintaining ROS equilibrium and enhancing adaptation to seed stress. Future research is needed to investigate the interaction mechanisms between OsNAT9 and other proteins involved in AsA metabolism, as well as the potential applications of this protein in enhancing crop stress tolerance through breeding.

OsNAT9 is required for drought tolerance in rice

Drought is a major abiotic stress that reduces crop yield. Under drought stress, the accumulation of ROS in plant cells increases markedly, leading to oxidative stress damage to cell membranes (reflected in MDA concentration), proteins, and DNA, thereby affecting plant growth and development (Xiong et al., 2018). AsA, an essential antioxidant in plants, plays an essential role in the regulation of plant adaptation to drought stress (Farooq et al., 2013). Research has demonstrated that overexpression of the *AtDHAR* gene in tobacco significantly elevates AsA concentration, thereby enhancing the drought tolerance of plants (Eltayeb et al., 2006). Moreover, the microRNA miR171i-*SCARECROW-LIKE PROTEINS26.1* module positively regulates the expression of the apple *MsMDHAR* gene, regulating the AsA metabolic pathway and consequently improving the drought tolerance of apple (Wang et al., 2020). In the present study, we elucidated the molecular mechanism by which the *OsNAT9* gene regulates drought tolerance in rice. The findings indicated that knockout of *OsNAT9* gene significantly lowered the drought tolerance of rice, whereas the overexpression of *OsNAT9* substantially enhanced drought tolerance (Figure 6A,B). Further analysis revealed that ROS accumulation and MDA concentration were significantly elevated in *Osnat9* mutants under drought stress compared with the wild-type and *OsNAT9-OE* lines (Figure 6C–F). Furthermore, knockout of the *OsNAT9* gene led to a significant reduction in AsA concentration in young leaves, whereas overexpression of the *OsNAT9* gene resulted in a notable increase in AsA concentration (Figure 6J). The accumulation of AsA not only facilitates the effective scavenging of ROS and reduces the MDA concentration in plants under drought stress but also promotes the accumulation of osmoregulatory substances, such as proline and soluble sugars (Akram et al., 2017; Chen & Gallie, 2005; Shalata & Neumann, 2001). These changes enhance the water retention capacity of plants and maintain cell turgor pressure, thereby mitigating mechanical damage induced by drought stress (Akram et al., 2017, Chen & Gallie, 2005, Shalata & Neumann, 2001). Interestingly, the overexpression of the *OsNAT9* gene exhibited differential effects on responses to seed aging and drought in rice. This seemingly contradictory phenomenon may be related to the different roles of *OsNAT9* in different tissues (Figure 5A). Seed aging reduces APX and glutathione reductase activity in the AsA-GSH cycle and the GSH/oxidized glutathione (GSSG) ratio, leading to ROS accumulation and oxidative damage in the embryo, which adversely affects seed germination and seedling growth (Chhabra & Singh, 2019). During seed aging, excessive efflux of AsA occurred in *OsNAT9-OE* lines embryos and the activity of key enzymes (such as APX) in the ASA-GSH cycle reduced by aging, resulting in the failure of AsA to be generated in a timely manner and a reduction in intracellular AsA concentration. This results in an accumulation of intracellular ROS, ultimately causing oxidative stress damage to the seed embryos (Figure 3E–K). Unlike seed aging, the *de novo* biosynthesis and recycling pathways of AsA in leaves and other plant organs may be more active in the overexpressed lines, thereby promoting rapid AsA biosynthesis or transport to leaves and enhancing the drought tolerance of rice plants (Figure S8). Nonetheless, the molecular mechanisms underlying AsA metabolism under these distinct stress conditions require further elucidation.

MATERIALS AND METHODS

Plant materials and growth conditions

The rice varieties utilized in this study, namely, TNG67, FXZ, and H603, were maintained at the Rice Research Institute, Fujian Academy of Agricultural Sciences, Fuzhou, Fujian Province, China. TNG67 served as the host plants for *A. tumefaciens*-mediated transformation to produce *OsNAT9-OE* lines and *Osnat9* mutants. The rice plants were grown in an experimental field at the Rice Research Institute, Fujian Academy of Agricultural Sciences. Upon reaching maturity, the rice seeds were harvested and subsequently dried at 42°C for 7 days to break seed dormancy. For in vitro culture on solid medium, the rice seeds were germinated on half-strength Murashige and Skoog (1/2MS) medium (Sigma-Aldrich). In hydroponic cultures, 10-day-old rice seedlings were transferred from 1/2MS agar plates to Hoagland's solution (Sigma-Aldrich). All rice seedlings were cultivated in a growth chamber under 14-h light and 10-h dark cycle at a temperature of 28 ± 1°C and 65% humidity.

Sequence alignment and phylogenetic analysis

Homologous proteins were identified using BLAST searches on the NCBI (https://blast.ncbi.nlm.nih.gov) and GBI websites (https://phytozome.jgi.doe.gov), employing the amino acid sequence of OsNAT9 as a query. Multiple sequence alignment of the NAT proteins was performed using ClustalW in MEGA 7 software (https://www.megasoftware.net/) and visualized with

GeneDoc software (Sun et al., 2016). A neighbor-joining (NJ) phylogenetic tree of NATs was constructed using MEGA 7 software, with the bootstrap value set to 1000.

RNA isolation and gene expression analysis

Fourteen-day-old TNG67 rice seedlings were subjected to various treatments, including 2.4 mM AsA, 100 μM ABA, 100 μM SA, 100 μM JA, 150 mM NaCl, 20 mM H_2O_2, 25% PEG6000, or distilled water. Approximately, 60 seedlings were selected for each experimental treatment, which was conducted with three biological replicates. Leaf samples were collected at baseline (0 h) and at 2, 4, 8, 12, 24, and 36 h post-treatment. These samples were immediately frozen in liquid nitrogen and stored at −80°C prior to RNA extraction.

Total RNA was extracted using TRIzol reagent (Thermo Fisher Scientific), and first-strand cDNA synthesis was performed using ReverTra Ace™ qPCR RT Master Mix with gDNA Remover (Toyoba). Quantitative real-time PCR (qPCR) was conducted using the 2 × FastStart Universal SYBR Green Master (Rox) reagent (Roche) on the LightCycler 480 II real-time fluorescent quantitative PCR instrument (Roche), with the rice *OsActin150* gene serving as the internal control. The primers utilized for the qPCR are detailed in Table S1. Data analysis was carried out using the LightCycler 480 II software (Roche). Each experiment was performed using three biological replicates.

Plasmid construction and plant transformation

The *Osnat9* knockout mutants of the TNG67 rice cultivar were generated utilizing the CRISPR-Cas9 system, following the procedure previously described (Wang, Xu, et al., 2023). For promoter expression analysis, a 2258-bp fragment upstream of the *OsNAT9* start codon was amplified using KOD DNA polymerase (Toyobo), and subsequently cloned into the pRHE-GUS plasmid via *Kpn*I and *Hind*III restriction sites, resulting in the construction of the pRHE-*proOsNAT9::GUS* vector. To achieve overexpression, the full-length *OsNAT9* coding sequence, without stop codons, was cloned into the pRHVcGFP plasmid using *Kpn*I and *Hind*III restriction sites to generate the pRHV-*proOsUbi::OsNAT9-GFP* vector. These constructed vectors were introduced into the TNG67 rice cultivar through *A. tumefaciens*-mediated transformation. The transgenic lines were confirmed by PCR and sequencing of genomic DNA. All experiments were conducted using homozygous lines from the T_3 generation.

Site-specific mutagenesis was employed to introduce point mutations into the OsNAT9 protein, generating the $OsNAT9^{S344A}$, $OsNAT9^{E346A}$, and $OsNAT9^{G349A}$ variants, as previously reported (Wang, He, et al., 2023). For protoplast AsA secretion and MST assays, the full-length *OsNAT9* gene and its mutant forms were cloned into the pYBA1132 vector via *Sal*I and *Eco*RI restriction sites. Table S1 presents the primer information used for vector construction.

Histochemical staining

To assess the promoter activity of *proOsNAT9*, GUS staining was performed on various organs from *proOsNAT9::GUS* transgenic plants, using a GUS staining solution kit (Sigma-Aldrich) in accordance with the manufacturer's instructions. Post-staining, the tissues were decolorized in 75% ethanol to facilitate imaging. ROS accumulation was evaluated using DAB and NBT staining. For DAB staining, leaf samples were subjected to vacuum infiltration in 1 mg/mL DAB staining solution (Solarbio) for 30 min, followed by incubation at 37°C in the dark overnight. For NBT staining, seeds and leaves were immersed in 0.2% (v/v) NBT solution (Solarbio) in the dark overnight. Imaging was performed using a TCS SP8 STED 3X laser confocal microscope (Leica) with laser excitation at 488 nm and emission at 535 nm for GFP, and laser excitation at 515 nm with emission ranging from 640 to 670 nm for FM4-64. For starch grain observation, seeds from *Osnat9* mutants, *OsNAT9-OE* lines, and the wild-type parent were transversely sectioned. The cross-sections of the seed endosperm were examined using a scanning electron microscope (Hitachi S-3500 N) and subsequently photographed with a Nikon SMZ800N stereo microscope equipped with a Nikon DS-Fi3 camera.

Seed vigor evaluation and artificial aging treatment

The assessment of seed germination was conducted following an established method (Wang, He, et al., 2023). For the artificial aging treatment, seeds of *Osnat9* mutants, *OsNAT9-OE* lines, and the wild-type parent were incubated in a ventilated heating chamber (Binder GmbH) for durations of 0, 7, 14, or 21 days under conditions of 42°C and 88% relative humidity. Either aged or unaged seeds of each genotype were placed in Petri dishes (9 cm in diameter) containing 10 mL of distilled water and incubated under a 14-h light/10-h dark cycle at 28 ± 1°C and 65% relative humidity for 7 days. Germination capacity was subsequently assessed. Germination was defined as the emergence of the radicle (length exceeding 2 mm) through the seed hull. Seedlings were considered developed when the root length equaled the seed length and the shoot length reached half of the seed length (Yang et al., 2022). Germination potential (GP), germination rate (GR), and germination index (GI) were calculated as described in a previous report (He et al., 2022). GP (%) = (Number of seeds germinated in 3 days after 24 h of imbibition/Total number of seeds) × 100. GR Calculation: GR (%) = (Number of seeds germinated in 7 days after 24 h of imbibition/Total number of seeds) × 100, and GI = ∑(Gt/t), where Gt represents the number of germinated seeds on a specific day and it is the total number of days the fifth day of germination test (He et al., 2022). For each experiment, all genotypes were evaluated, with three biological replicates performed for each genotype. Each replicate contains 50 seeds (Pang et al., 2022).

Evaluation of the drought tolerance

The germinated seeds of *Osnat9* mutants, *OsNAT9-OE*, and the wild-type lines were transplanted into pots and cultivated for 3 weeks using Hoagland's nutrient solution. Subsequently, the seedlings were subjected to Hoagland's nutrient solution (Sigma-Aldrich) supplemented with 25% (v/v) PEG6000 for an additional 3 weeks to simulate drought stress. Upon observing complete leaf rolling, the seedlings were transferred back to Hoagland's nutrient solution for recovery period of 7 days. The survival rates for each sample were determined by calculating the ratio of the number of surviving plants per pot to the total number of treated plants in the pot.

Redox status analysis

To assess the redox status of seeds and leaves in wild-type, *OsNAT9-OE* lines, and *Osnat9* mutants subjected to artificial aging and drought stress, we measured the activities of antioxidant enzymes, including SOD, POD, CAT, and APX. Additionally, the levels of MDA and H^2O^2 were quantified. All assays were conducted in accordance with the manufacturer's instructions accompanying the assay kits (Solarbio), and each experiment was replicated a minimum of three times.

Metabolomics analysis

The extraction method for seed embryo metabolites was adapted from a previously established protocol (Pang et al., 2022). Embryos from both wild-type and *Osnat9* mutant seeds were harvested at intervals of 0, 7, and 14 days following artificial aging. Each group of experiments included three biological replicates. These samples were subsequently frozen in liquid nitrogen and ground into powder. A subsample (50 mg) of the resultant powder was transferred into a 1.5 mL centrifuge tube, and 1.2 mL of 70% (v/v) methanol was added. The mixture was shaken to ensure thorough mixing, followed by centrifugation at 13400 g for 3 min to separate the phases. The supernatant was then collected and filtered through a 0.22-μm membrane filter. The filtered extract was analyzed for metabolite content using ultra-high-performance liquid chromatography–tandem mass spectrometry (UPLC-MS/MS) with the ACQUITY UPLC H-Class system (Waters Corp.), which was equipped with an Agilent SB-C18 column (2.1 × 100 mm, 1.8 μm particle size). The chromatographic separation was achieved using gradient elution with solvent A, comprising ultra-pure water containing 0.1% (v/v) formic acid, and solvent B, consisting of acetonitrile containing 0.1% (v/v) formic acid. The gradient program was as follows: from 0 to 9 min, the proportion of solvent B was increased from 5% to 95%; from 9 to 10 min, it was maintained at 95%; and from 10 to 11 min, it was reduced back to 5% and held constant until 14 min. The flow rate was maintained at 0.35 mL/min, with the column temperature set at 35°C, and a sample injection volume of 5 μL was used.

Mass spectrometry was conducted under the following conditions: the electrospray ionization source temperature was set at 550°C, with ion spray voltages of 5500 V for positive ion mode and-4500 V for negative ion mode. The ion source gas I, gas II, and gas curtain gas were set at 50 psi, 60 psi, and 25 psi, respectively, with collision-induced dissociation parameters adjusted to "high." The scan mode employed was multiple reaction monitoring (MRM), utilizing nitrogen as the collision gas. The declustering potential and collision energy were optimized for each metabolite. A specific set of MRM ion pairs was monitored during each period, corresponding to the elution profile of the metabolites.

Based on the self-established database Metware (https://www.metwarebio. com/) and a public database of metabolite information (https://www.metabolomicsworkbench.org), the samples were qualitatively and quantitatively analyzed using MS/MS.

Seed germination analysis following AsA treatment

Thirty seeds each of the *Osnat9* mutants, the *OsNAT9-OE* lines, and the wild-type parent were surface-sterilized and sown on 1/2 MS medium supplemented with 0, 0.3, 0.6, 1.2, or 2.4 mM AsA for germination assessment. The experiment was conducted with three biological replicates. Seeds were incubated under a 14-h light/10-h dark cycle at 30°C and 80% relative humidity, with a light intensity of 100 $\mu mol \cdot m^{-2} \cdot s^{-1}$. The number of germinated seeds was recorded daily, and GP, GR, and GI were measured and calculated on the sixth day.

Protoplast AsA secretion assay

The isolation of rice protoplasts was conducted following a previously established protocol with slight modifications (Zhang et al., 2011). Seeds from the *Osnat9* mutants, *OsNAT9-OE* lines, and wild-type rice were subjected to surface sterilization using 75% (v/v) ethanol, subsequently rinsed with sterile water, and incubated in sterile water at 26°C under a 12-h light (at 150 $\mu mol \cdot m^{-2} \cdot s^{-1}$) and 12-h dark cycle for a duration of 10–14 days. Green tissues from the stems and leaf sheaths of 40–60 rice seedlings were excised into 0.5 mm length strips and incubated in 0.6 M mannitol solution in darkness for 10 minutes. The tissue strips were then transferred to an enzyme solution (1.5% cellulase RS, 0.5% macerozyme R-10, 0.5 M mannitol, 10 mM MES, pH 5.7, 3.4 mM $CaCl^2$, 50 μg/mL carbenicillin, and 0.1% bovine serum albumen [BSA]) and subjected to gentle agitation in the dark for 4 h. After enzymatic digestion, an equivalent volume of W5 solution (154 mM NaCl, 125 mM $CaCl^2$, 5 mM KCl, 2 mM MES, pH 5.7) was added, and the mixture was vigorously shaken for 10 sec. Protoplasts were subsequently released by filtration through a 40-μm nylon mesh, washed with W5 solution, and collected by centrifugation at 150 g for 3 min. The resulting pellet was resuspended in MMG solution (0.4 M mannitol, 15 mM $MgCl^2$, 4 mM MES, pH 5.7) to achieve a concentration of 1×10^6 protoplasts/mL. Protoplasts were cultured in W5 solution with varying concentrations of DHA (0, 5, 25, or 50 mM) in darkness for 16 h. Subsequently, the W5 solution and protoplasts were collected for the assessment of AsA concentration.

UPLC measurement of AsA concentration

The extraction of AsA was performed according to previously reported methods (Wang, He, et al., 2023). Plant tissues were collected, freeze-dried, and subsequently weighed and ground into powder. The powder was then transferred into 1.5 mL centrifuge tubes. The extraction process involved the use of 5% (w/v) trichloroacetic acid (TCA), followed by centrifugation at 7000*g* for 10 min at 4°C. The resultant supernatant was collected and filtered through a 0.45-μm membrane filter for subsequent analysis. Protoplasts were separated via centrifugation at 1.50 g for 3 min at room temperature, and the culture medium was similarly filtered through a 0.45-μm membrane filter for further examination. The protoplasts underwent washing with W5 solution and were extracted using 5% TCA. The supernatant was collected and centrifuged at 7000*g* for 10 min at 4°C. The supernatant was collected and filtered through a 0.45-μm membrane filter for future use. The AsA content was quantified using ultra-high-performance liquid chromatography (UPLC) on a Waters ACQUITY UPLC H-Class system, equipped with an HSS T3 column (2.1 × 150 mm, 1.8 μm). The mobile phase comprised solvent A (water containing 0.1% formic acid) and solvent B (acetonitrile). The gradient elution program was as follows: from 0 to 6.5 min, solvent B increased from 8% to 50%; from 6.5 to 10 min, solvent B returned to 8%; and from 10 to 12 min, solvent B was maintained at 8%. The flow rate was set at 0.2 mL/min, the column temperature was maintained at 30°C, the sample injection volume was 2.0 μL, and the detection wavelength was set at 243 nm.

Protein expression and purification

The GFP-tagged control vector, *OsNAT9*, or *OsNAT9* variants $OsNAT9^{S344A}$, $OsNAT9^{E346A}$, and $OsNAT9^{G349A}$ plasmids in pYBA1132 vectors were transiently expressed in protoplasts derived from the rice cultivar Nipponbare, utilizing a PEG-mediated transfection method. After a 16-h incubation period, the protoplasts were harvested by centrifugation at 150*g* for 3 min, followed by protein extraction. The protoplasts were resuspended in an immunoprecipitation buffer (IP-buffer), containing 50 mM Tris–HCl, pH 7.5, 150 mM NaCl, 0.1% (v/v) Triton-100, 5 mM $CaCl^2$, 0.1 mM phenylmethanesulfonyl fluoride, and 10% (v/v) glycerol, and subsequently homogenized by sonication on ice. Anti-GFP agarose beads (Beijing LABLEAD Trading Co., Ltd) were pre-equilibrated with the IP-buffer. The proteins were incubated with

the anti-GFP agarose beads at room temperature for 1 h to facilitate the adsorption of target proteins, while impurities were removed by seven washes with the IP-buffer. The GFP fusion proteins were eluted from the beads using 0.2 M glycine (pH 2.5) followed by neutralization with 1.0 M Tris (pH 10.4). The purified proteins were subsequently collected for further analysis. The abundance of GFP-tagged OsNAT9 proteins was analyzed by quantifying the total fluorescence of GFP.

Microscale thermophoresis analysis

MST was employed to confirm protein–ligand interactions, as previously described (Zhang et al., 2011). MST analysis of the interaction between ascorbic acid and OsNAT9 was performed using the Monolith NT.115 instrument (Nanotemper). For the binding studies, the purified proteins GFP control protein or OsNAT9 variants OsNAT9-GFP, OsNAT9^{S344A}-GFP, OsNAT9^{E346A}-GFP, and OsNAT9^{G349A}-GFP proteins were diluted fourfold with IP-buffer to optimize the fluorescent protein concentration for the binding reaction. The compound was titrated with IP-buffer at a 1:1 ratio and subsequently diluted 16-fold. Thereafter, 5 μL of the diluted protein was mixed with 5 μL of ascorbic acid or xanthine in varying concentrations. Following a 5-min incubation period at room temperature, all samples were introduced into Monolith NT.115 capillaries (Nanotemper), using 50% IR laser power and an LED excitation source (λ = 470 nm) at 25°C. Each experiment was repeated at least three times independently. The data were analyzed using Nanotemper Analysis 1.2.20 software to determine the dissociation constant (K_d) using the K_d model (Yang et al., 2023).

Data analysis

The experimental data were analyzed utilizing SPSS Statistics v. 26 (IBM). Significant differences among the samples were determined through the application of Student's *t*-test or analysis of variance (ANOVA) followed by pairwise multiple comparisons using Fisher's least significant difference (LSD) test, with significance levels set at 5%, 1%, and 0.1%. The results were expressed as mean ± standard deviation. Data organization and diagrammatic representation were accomplished using GraphPad Prism version 6.01(GraphPad Software Inc), Adobe Photoshop CS6 (Adobe Systems Inc.), and TB-tools version 2.012 (https://github.com/CJ-Chen/TBtools_tbtools).

AUTHOR CONTRIBUTIONS

SFL, HAX, and JFZ: conceptualization, supervision, investigation, formal analysis, visualization, and writing – original draft. KYL, YDW, and SZ: investigation and validation. MZ, JHJ, JLW, TC, FXW, and JXF: investigation. QHC, YHW, LPC, WH, HAX, and JFZ: conceptualization, supervision, writing – review and editing, and funding acquisition.

ACKNOWLEDGMENTS

This work was conducted at Rice Research Institute, Fujian Academy of Agricultural Sciences. The work was supported by the National Rice Industry Technology System of Modern Agriculture for China (grant no. CARS-01-20), the "5511" Collaborative Innovation Project for High-quality Development and Surpasses of Agriculture between the Government of Fujian and Chinese Academy of Agricultural Sciences (grant no. XTCXGC2021001) and the Special Foundation of Non-Profit Research Institutes of Fujian Province (grant no. 2020R1023008). We sincerely appreciate the generous assistance of Researcher Shang Lianguang from the Shenzhen Institute of Agricultural Genomics, Chinese Academy of Agricultural Sciences, in helping us analyze 251 high-quality rice genomes for our research.

CONFLICT OF INTEREST

No conflict of interest was declared.

DATA AVAILABILITY STATEMENT

The data that support the findings of this study are available on request from the corresponding author. The data are not publicly available due to privacy or ethical restrictions.

SUPPORTING INFORMATION

Additional Supporting Information may be found in the online version of this article.

Table S1. Primer sequences used in this study.

Figure S1. Structural analysis of OsNAT9 in plants.

Figure S2. Hierarchical cluster analysis of significantly changed proteins classified as being involved in embryos of "H603" and "FXZ" seeds exposed to artificial aging.

Figure S3. Alignment of the NAT protein sequences from different organisms.

Figure S4. Seed germination after breaking dormancy at 42°C and 88% humidity for 7 days.

Figure S5. Comparison of seed vigor in *Oryza sativa* among wild-type "TNG67," the *Osnat9* mutants, and *OsNAT9-OE* lines after natural aging for 6 months.

Figure S6. KEGG enrichment analysis of the DAMs in embryos between wild-type "TNG67" and *Osnat9* mutants after 7 and 14 days of artificial aging.

Figure S7. Exogenous AsA treatment promoted the germination of *OsNAT9* knockout seeds.

Figure S8. The expression levels of genes involved in ASA *de novo* biosynthesis or recycling pathways in different organs.

REFERENCES

Akram, N.A., **Shafiq, F.** & **Ashraf, M.** (2017) Ascorbic acid - a potential oxidant scavenger and its role in plant development and abiotic stress tolerance. *Frontiers in Plant Science*, **8**, 613.

Argyrou, E., **Sophianopoulou, V.**, **Schultes, N.** & **Diallinas, G.** (2001) Functional characterization of a maize purine transporter by expression in *aspergillus nidulans*. *The Plant Cell*, **13**, 953–964.

Bewley, J.D. (1997) Seed germination and dormancy. *The Plant Cell*, **9**, 1055–1066.

Broad, R.C., **Bonneau, J.P.**, **Hellens, R.P.** & **Johnson, A.A.** (2020) Manipulation of ascorbate biosynthetic, recycling, and regulatory pathways for improved abiotic stress tolerance in plants. *International Journal of Molecular Sciences*, **21**, 1790.

Celi, G.E.A., **Gratão, P.L.**, **Lanza, M.G.D.B.** & **Dos Reis, A.R.** (2023) Physiological and biochemical roles of ascorbic acid on mitigation of abiotic stresses in plants. *Plant Physiology and Biochemistry*, **202**, 107970. Available from: https://doi.org/10.1016/j.plaphy.2023.107970

Chen, W., **Hu, T.**, **Ye, J.**, **Wang, B.**, **Liu, G.**, **Wang, Y.** ***et al.*** (2020) A CCAAT-binding factor, SlNFYA10, negatively regulates ascorbate accumulation by modulating the D-mannose/L-galactose pathway in tomato. *Horticulture Research*, **7**, 200.

Chen, Z. & **Gallie, D.R.** (2005) Increasing tolerance to ozone by elevating foliar ascorbic acid confers greater protection against ozone than increasing avoidance. *Plant Physiology*, **138**, 1673–1689.

Chhabra, R. & **Singh, T.** (2019) Seed aging, storage and deterioration: an irresistible physiological phenomenon. *Agricultural Reviews*, **40**, 234–238.

Conklin, P.L., **Norris, S.R.**, **Wheeler, G.L.**, **Williams, E.H.**, **Smirnoff, N.** & **Last, R.L.** (1999) Genetic evidence for the role of GDP-mannose in plant ascorbic acid (vitamin C) biosynthesis. *Proceedings of the National Academy of Sciences*, **96**, 4198–4203.

Conklin, P.L., **Pallanca, J.E.**, **Last, R.L.** & **Smirnoff, N.** (1997) L-ascorbic acid metabolism in the ascorbate-deficient *Arabidopsis* mutant *vtc1*. *Plant Physiology*, **115**, 1277–1285.

Conklin, P.L., **Williams, E.H.** & **Last, R.L.** (1996) Environmental stress sensitivity of an ascorbic acid-deficient Arabidopsis mutant. *Proceedings of the National Academy of Sciences*, **93**, 9970–9974.

Debeaujon, I. & **Koornneef, M.** (2000) Gibberellin requirement for *Arabidopsis* seed germination is determined both by testa characteristics and embryonic abscisic acid. *Plant Physiology*, **122**, 415–424.

Eltayeb, A.E., **Kawano, N.**, **Badawi, G.H.**, **Kaminaka, H.**, **Sanekata, T.**, **Morishima, I.** ***et al.*** (2006) Enhanced tolerance to ozone and drought stresses in transgenic tobacco overexpressing dehydroascorbate reductase in cytosol. *Physiologia Plantarum*, **127**, 57–65.

Farooq, M., **Irfan, M.**, **Aziz, T.**, **Ahmad, I.** & **Cheema, S.** (2013) Seed priming with ascorbic acid improves drought resistance of wheat. *Journal of Agronomy and Crop Science*, **199**, 12–22.

Fitzgerald, M.A., **McCouch, S.R.** & **Hall, R.D.** (2009) Not just a grain of rice: the quest for quality. *Trends in Plant Science*, **14**, 133–139.

Foyer, C.H. & **Halliwell, B.** (1976) The presence of glutathione and glutathione reductase in chloroplasts: a proposed role in ascorbic acid metabolism. *Planta*, **133**, 21–25.

Foyer, C.H. & **Noctor, G.** (2011) Ascorbate and glutathione: the heart of the redox hub. *Plant Physiology*, **155**, 2–18.

Gallie, D.R. (2013) The role of L-ascorbic acid recycling in responding to environmental stress and in promoting plant growth. *Journal of Experimental Botany*, **64**, 433–443.

He, C., **Deng, F.**, **Yuan, Y.**, **Huang, X.**, **He, Y.**, **Li, Q.** ***et al.*** (2024) Appearance, components, pasting, and thermal characteristics of chalky grains of rice varieties with varying protein content. *Food Chemistry*, **440**, 138256.

He, Y., **Chen, S.**, **Liu, K.**, **Chen, Y.**, **Cheng, Y.**, **Zeng, P.** ***et al.*** (2022) OsHIPL1, a hedgehog-interacting protein-like 1 protein, increases seed vigour in rice. *Plant Biotechnology Journal*, **20**(7), 1346–1362. Available from: https://doi.org/10.1111/pbi.13812

Hoang, M.T.T., **Almeida, D.**, **Chay, S.**, **Alcon, C.**, **Corratge-Faillie, C.**, **Curie, C.** ***et al.*** (2021) AtDTX25, a member of the multidrug and toxic compound extrusion family, is a vacuolar ascorbate transporter that controls intracellular iron cycling in *Arabidopsis*. *New Phytologist*, **231**, 1956–1967.

Horemans, N., **Foyer, C.H.** & **Asard, H.** (2000) Transport and action of ascorbate at the plant plasma membrane. *Trends in Plant Science*, **5**, 263–267.

Ishikawa, T., **Maruta, T.**, **Yoshimura, K.** & **Smirnoff, N.** (2018) Biosynthesis and regulation of ascorbic acid in plants. *Antioxidants and Antioxidant Enzymes in Higher Plants*, 163–179.

Kerk, N.M. & **Feldman, L.J.** (1995) A biochemical model for the initiation and maintenance of the quiescent center: implications for organization of root meristems. *Development*, **121**, 2825–2833.

Koornneef, M., **Jorna, M.**, **Van der Brinkhorst- Swan, D.** & **Karssen, C.** (1982) The isolation of abscisic acid (ABA) deficient mutants by selection of induced revertants in non-germinating gibberellin sensitive lines of *Arabidopsis thaliana* (L.) Heynh. *Theoretical and Applied Genetics*, **61**, 385–393.

Kosti, V., **Lambrinidis, G.**, **Myrianthopoulos, V.**, **Diallinas, G.** & **Mikros, E.** (2012) Identification of the substrate recognition and transport pathway in a eukaryotic member of the nucleobase-ascorbate transporter (NAT) family. *PLoS One*, **7**, e41939.

Lima, R.B., **Pankaj, R.**, **Ehlert, S.T.**, **Finger, P.**, **Fröhlich, A.**, **Bayle, V.** ***et al.*** (2024) Seed coat-derived brassinosteroid signaling regulates endosperm development. *Nature Communications*, **15**, 9352.

Liu, Y., **Bergervoet, J.H.**, **De Vos, C.R.**, **Hilhorst, H.W.**, **Kraak, H.L.**, **Karssen, C.M.** ***et al.*** (1994) Nuclear replication activities during imbibition of abscisic acid-and gibberellin-deficient tomato (*Lycopersicon esculentum* mill.) seeds. *Planta*, **194**, 368–373.

Mittler, R. (2002) Oxidative stress, antioxidants and stress tolerance. *Trends in Plant Science*, **7**, 405–410.

Miyaji, T., **Kuromori, T.**, **Takeuchi, Y.**, **Yamaji, N.**, **Yokosho, K.**, **Shimazawa, A.** ***et al.*** (2015) AtPHT4; 4 is a chloroplast-localized ascorbate transporter in *Arabidopsis*. *Nature Communications*, **6**, 5928.

Niu, J., **Xu, M.**, **Zong, N.**, **Sun, J.**, **Zhao, L.** & **Hui, W.** (2024) Ascorbic acid releases dormancy and promotes germination by an integrated regulation of abscisic acid and gibberellin in Pyrus betulifolia seeds. *Physiologia Plantarum*, **176**, e14271.

Oenel, A., **Fekete, A.**, **Krischke, M.**, **Faul, S.C.**, **Gresser, G.**, **Havaux, M.** ***et al.*** (2017) Enzymatic and non-enzymatic mechanisms contribute to lipid oxidation during seed aging. *Plant and Cell Physiology*, **58**, 925–933.

Padh, H. (1990) Cellular functions of ascorbic acid. *Biochemistry and Cell Biology*, **68**, 1166–1173.

Pang, X., **Suo, J.**, **Liu, S.**, **Xu, J.**, **Yang, T.**, **Xiang, N.** ***et al.*** (2022) Combined transcriptomic and metabolomic analysis reveals the potential mechanism of seed germination and young seedling growth in Tamarix hispida. *BMC Genomics*, **23**(1), 109–124. Available from: https://doi.org/10.1186/s12864-022-08341-x

Pignocchi, C. & **Foyer, C.H.** (2003) Apoplastic ascorbate metabolism and its role in the regulation of cell signalling. *Current Opinion in Plant Biology*, **6**, 379–389.

Shalata, A. & **Neumann, P.M.** (2001) Exogenous ascorbic acid (vitamin C) increases resistance to salt stress and reduces lipid peroxidation. *Journal of Experimental Botany*, **52**, 2207–2211.

Singh, V.P., **Jaiswal, S.**, **Wang, Y.**, **Feng, S.**, **Tripathi, D.K.**, **Singh, S.** ***et al.*** (2024) Evolution of reactive oxygen species cellular targets for plant development. *Trends in Plant Science*, **29**, 865–877.

Solberg, S.Ø., **Yndgaard, F.**, **Andreasen, C.**, **Von Bothmer, R.**, **Loskutov, I.G.** & **Asdal, Å.** (2020) Long-term storage and longevity of orthodox seeds: a systematic review. *Frontiers in Plant Science*, **11**, 1007.

Sun, T., **Jia, D.**, **Huang, L.**, **Shao, Y.** & **Ma, F.** (2016) Comprehensive genomic identification and expression analysis of the nucleobase-ascorbate transporter (NAT) gene family in apple. *Scientia Horticulturae*, **198**, 473–481.

Tóth, D., **Tengölics, R.**, **Aarabi, F.**, **Karlsson, A.**, **Vidal-Meireles, A.**, **Kovács, L.** ***et al.*** (2024) Chloroplastic ascorbate modifies plant metabolism and may act as a metabolite signal regardless of oxidative stress. *Plant Physiology*, **196**, 1691–1711.

Wang, F., **Xu, H.**, **Zhang, L.**, **Shi, Y.**, **Song, Y.**, **Wang, X.** ***et al.*** (2023) The lipoxygenase OsLOX10 affects seed longevity and resistance to saline-alkaline stress during rice seedlings. *Plant Molecular Biology*, **111**, 415–428.

Wang, H., **Qi, Q.**, **Schorr, P.**, **Cutler, A.J.**, **Crosby, W.L.** & **Fowke, L.C.** (1998) ICK1, a cyclin-dependent protein kinase inhibitor from Arabidopsis thaliana interacts with both Cdc2a and CycD3, and its expression is induced by abscisic acid. *The Plant Journal*, **15**, 501–510.

Wang, M., **He, J.**, **Li, S.**, **Cai, Q.**, **Zhang, K.** & **She, J.** (2023) Structural basis of vitamin C recognition and transport by mammalian SVCT1 transporter. *Nature Communications*, **14**, 1361.

Wang, W., **He, A.**, **Peng, S.**, **Huang, J.**, **Cui, K.** & **Nie, L.** (2018) The effect of storage condition and duration on the deterioration of primed rice seeds. *Frontiers in Plant Science*, **9**, 172.

Wang, Y., **Feng, C.**, **Zhai, Z.**, **Peng, X.**, **Wang, Y.**, **Sun, Y.** ***et al.*** (2020) The apple microR171i-SCARECROW-LIKE PROTEINS26. 1 module enhances drought stress tolerance by integrating ascorbic acid metabolism. *Plant Physiology*, **184**, 194–211.

Wheeler, G.L., **Jones, M.A.** & **Smirnoff, N.** (1998) The biosynthetic pathway of vitamin C in higher plants. *Nature*, **393**, 365–369.

Wu, B., **Yun, P.**, **Zhou, H.**, **Xia, D.**, **Gu, Y.**, **Li, P.** ***et al.*** (2022) Natural variation in WHITE-CORE RATE 1 regulates redox homeostasis in rice endosperm to affect grain quality. *The Plant Cell*, **34**, 1912–1932.

Wu, S.Y., **Hou, L.L.**, **Zhu, J.**, **Wang, Y.C.**, **Zheng, Y.L.**, **Hou, J.Q.** ***et al.*** (2023) Ascorbic acid-mediated reactive oxygen species homeostasis modulates the switch from tapetal cell division to cell differentiation in *Arabidopsis*. *The Plant Cell*, **35**, 1474–1495.

Xiong, H., **Yu, J.**, **Miao, J.**, **Li, J.**, **Zhang, H.**, **Wang, X.** ***et al.*** (2018) Natural variation in OsLG3 increases drought tolerance in rice by inducing ROS scavenging. *Plant Physiology*, **178**, 451–467.

Yang, B., **Chen, M.**, **Zhan, C.**, **Liu, K.**, **Cheng, Y.**, **Xie, T.** ***et al.*** (2022) Identification of OsPK5 involved in rice glycolytic metabolism and GA/ABA balance for improving seed germination via genome-wide association study. *Journal of Experimental Botany*, **73**, 3446–3461.

Yang, S., **Cai, W.**, **Wu, R.**, **Huang, Y.**, **Lu, Q.**, **Wang, H.** ***et al.*** (2023) Differential CaKAN3-CaHSF8 associations underlie distinct immune and heat responses under high temperature and high humidity conditions. *Nature Communications*, **14**, 4477.

Ye, T., **Ma, T.**, **Chen, Y.**, **Liu, C.**, **Jiao, Z.**, **Wang, X.** ***et al.*** (2024) The role of redox-active small molecules and oxidative protein post-translational modifications in seed aging. *Plant Physiology and Biochemistry*, **213**, 108810.

Yu, Y., **Wang, J.**, **Li, S.**, **Kakan, X.**, **Zhou, Y.**, **Miao, Y.** ***et al.*** (2019) Ascorbic acid integrates the antagonistic modulation of ethylene and abscisic acid in the accumulation of reactive oxygen species. *Plant Physiology*, **179**, 1861–1875.

Zhang, W., **Lorence, A.**, **Gruszewski, H.A.**, **Chevone, B.I.** & **Nessler, C.L.** (2009) AMR1, an *Arabidopsis* gene that coordinately and negatively regulates the mannose/l-galactose ascorbic acid biosynthetic pathway. *Plant Physiology*, **150**, 942–950.

Zhang, Y., **Su, J.**, **Duan, S.**, **Ao, Y.**, **Dai, J.**, **Liu, J.** ***et al.*** (2011) A highly efficient rice green tissue protoplast system for transient gene expression and studying light/chloroplast-related processes. *Plant Methods*, **7**, 1–14.

Zhao, X., **Guo, X.**, **Tang, X.**, **Zhang, H.**, **Wang, M.**, **Kong, Y.** ***et al.*** (2018) Misregulation of ER-Golgi vesicle transport induces ER stress and affects seed vigor and stress response. *Frontiers in Plant Science*, **9**, 658.

Zhou, H.X., **Milne, R.I.**, **Ma, X.L.**, **Song, Y.Q.**, **Fang, J.Y.**, **Sun, H.** ***et al.*** (2018) Characterization of a L-Gulono-1, 4-lactone oxidase like protein in the floral nectar of Mucuna sempervirens, Fabaceae. *Frontiers in Plant Science*, **9**, 1109. Available from: https://doi.org/10.3389/fpls.2018.01109

Ziada, A.S., **Smith, M.-S.R.** & **Côté, H.C.** (2020) Updating the free radical theory of aging. *Frontiers in Cell and Developmental Biology*, **8**, 575645.